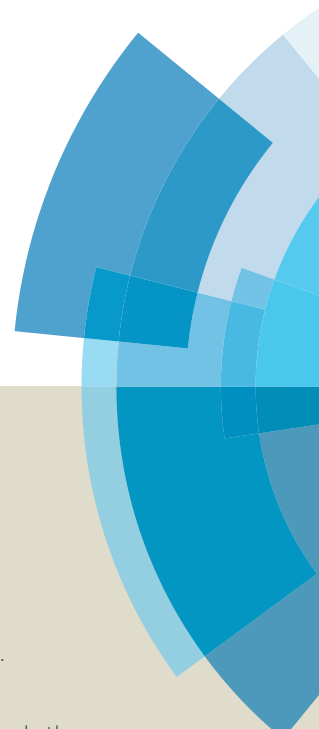
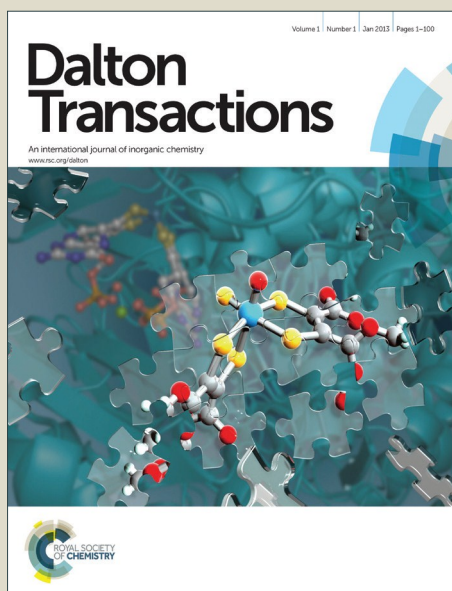


Dalton Transactions

Accepted Manuscript



This article can be cited before page numbers have been issued, to do this please use: B. M. Ahmed, B. Calco and G. Mezei, *Dalton Trans.*, 2016, DOI: 10.1039/C6DT00847J.



This is an *Accepted Manuscript*, which has been through the Royal Society of Chemistry peer review process and has been accepted for publication.

Accepted Manuscripts are published online shortly after acceptance, before technical editing, formatting and proof reading. Using this free service, authors can make their results available to the community, in citable form, before we publish the edited article. We will replace this *Accepted Manuscript* with the edited and formatted *Advance Article* as soon as it is available.

You can find more information about *Accepted Manuscripts* in the [Information for Authors](#).

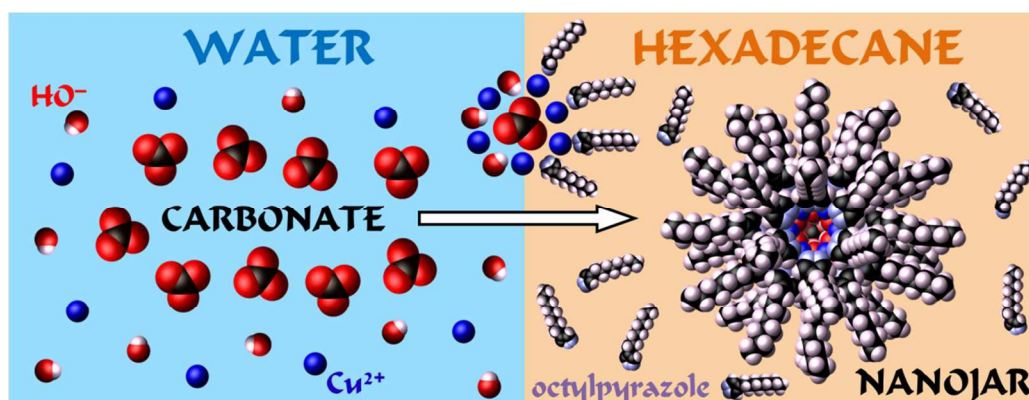
Please note that technical editing may introduce minor changes to the text and/or graphics, which may alter content. The journal's standard [Terms & Conditions](#) and the [Ethical guidelines](#) still apply. In no event shall the Royal Society of Chemistry be held responsible for any errors or omissions in this *Accepted Manuscript* or any consequences arising from the use of any information it contains.

Tuning the structure and solubility of nanojars by peripheral ligand substitution, leading to unprecedented liquid-liquid extraction of the carbonate ion from water into aliphatic solvents

Basil M. Ahmed, Brice Calco and Gellert Mezei*

Department of Chemistry, Western Michigan University, Kalamazoo, Michigan, USA

*Correspondent author. Email: gellert.mezei@wmich.edu



Carbonate, an anion with large hydration energy, is extracted from water by solvent extraction for the first time, using functionalized nanojars

ABSTRACT

Nanojars, a novel class of neutral anion-incarcerating agents of the general formula $[\text{Cu}^{\text{II}}(\text{OH})(\text{pz})]_n$ (Cu_n ; $n = 27\text{--}31$, $\text{pz} = \text{pyrazolate anion}$), efficiently sequester various oxoanions with large hydration energies from water. In this work, we explore whether substituents on the pyrazole ligand interfere with nanojar formation, and whether appropriate substituents could be employed to tune the solubility of nanojars in solvents of interest, such as long-chain aliphatic hydrocarbons (solvent of choice for large-scale liquid-liquid extraction processes) and water. To this end, we conducted a comprehensive study using 40 different pyrazole ligands, with one, two or three substituents in their 3-, 4- and 5-positions. The corresponding nanojars are characterized by single-crystal X-ray diffraction and/or electrospray-ionization mass spectrometry (ESI-MS). The results show that Cu_n -nanojars with various substituents in the pyrazole 4-position, including long chains, phenyl and CF_3 groups, can be obtained. Straight chains are also tolerated at the pyrazole 3-position, and favor the Cu_{30} -nanojar. Homoleptic nanojars, however, could not be

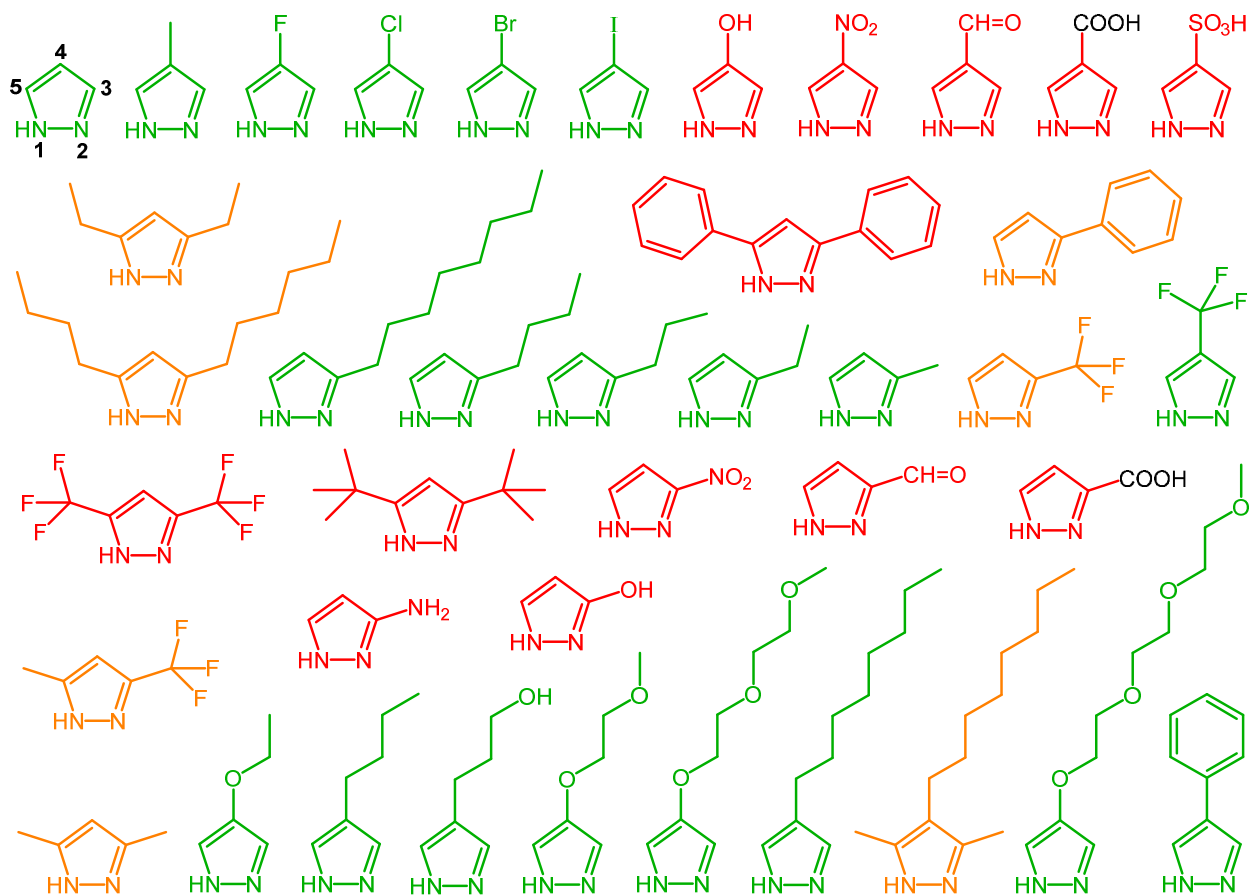
obtained with phenyl or CF₃ groups. Nevertheless, if used in mixture with the parent non-substituted pyrazole, sterically hindered pyrazoles do form heteroleptic nanojars. With 3,5-disubstituted pyrazoles, only heteroleptic nanojars are accessible. The crystal structure of novel nanojars (Bu₄N)₂[CO₃C{Cu₃₀(OH)₃₀(3,5-Me₂pz)_y(pz)_{30-y}}] (y = 14 and 15) is presented. We find that in contrast to the parent nanojar, which is insoluble in aliphatic solvents and water, nanojars with alkyl substituents are soluble in saturated hydrocarbon solvents, whereas nanojars based on novel pyrazoles, functionalized with oligoether chains, are readily soluble in water. Liquid-liquid extraction of carbonate from water under basic pH is presented for the first time.

1. INTRODUCTION

Nanojars constitute a unique, novel class of anion-sequestering agents of unparalleled efficiency.¹⁻³ Comprised of three-ring assemblies of [*cis*-Cu^{II}(μ-OH)(μ-pz)]_x metallamacrocycles (x = 6–14, except 11), these supramolecular coordination assemblies bind di- or trinegative anions, such as sulfate,^{1,3} phosphate,² arsenate² and carbonate,³ by wrapping a multitude of hydrogen bonds around and totally isolating the anion from its surrounding medium (as in the sulfate-⁴ and phosphate-binding proteins⁵). Various nanojars of the general formula (Bu₄N)₂[EO_a²⁻{Cu(OH)(pz)}_n] (E = C, a = 3; E = S, HP or HAs, a = 4; n = 27–31) have been discovered to date, containing the following ring-combinations: n = 6+12+9 (Cu₂₇), 6+12+10 (Cu₂₈), 7+13+9 (Cu₂₉), 8+13+8 (Cu₂₉) and 8+14+9 (Cu₃₁). The unprecedented anion-binding strength is demonstrated by the inability of an aqueous Ba²⁺ solution to precipitate barium sulfate, phosphate or arsenate, respectively, when stirred with a solution of the corresponding nanojars.^{1,2} Thus, nanojars could be exploited as highly efficient liquid-liquid extraction agents for the removal of those anions from contaminated aqueous media.

Currently, there is a strong interest in developing novel chemical systems for the recognition of anions, with an aim at efficient and selective removal and recovery of anions from solution,⁶⁻¹⁶ anion sensing,^{17,18} and anion transport.¹⁹⁻²³ Anions with large hydration energies, such as PO₄³⁻ (ΔG_h^o = -2773 kJ mol⁻¹), CO₃²⁻ (ΔG_h^o = -1315 kJ mol⁻¹) and SO₄²⁻ (ΔG_h^o = -1090 kJ mol⁻¹),²⁴ are particularly difficult to extract from aqueous solutions, and to the best of our knowledge, no liquid-liquid extraction method of carbonate is known. Nanojars based on the parent pyrazole ligand bind carbonate strongly; however, these nanojars are not soluble in organic solvents suitable for industrial-scale liquid-liquid extraction processes, *i.e.* long-chain

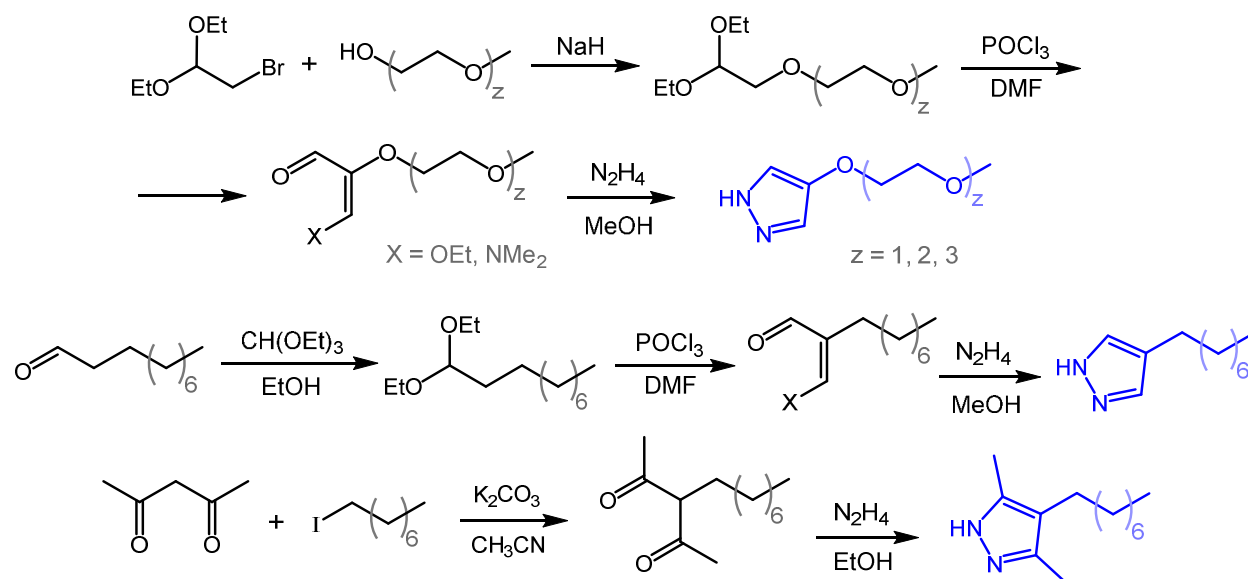
aliphatic hydrocarbons. To address this issue, as well as to study the effect of pyrazole substituents on the structure and stability of nanojars, we conducted a comprehensive study using 40 different pyrazole ligands with either one, two or three substituents in their 3-, 4- and 5-positions (Scheme 1). The novel nanojars are characterized by single-crystal X-ray diffraction in the solid state, and/or electrospray-ionization mass spectrometry (ESI-MS) in solution. The structure of two different Cu_{30} -nanojars are described for the first time, which are comprised of previously unknown ring combinations, $n = 8+14+8$ and $n = 7+14+9$. Peripheral decoration of the nanojars with long hydrocarbon or oligoether chains expands the solubility of nanojars to aliphatic solvents and water, respectively. For this purpose, novel pyrazole ligands with oligo(ethylene glycol) methyl ether substituents have been synthesized. Furthermore, we use highly hydrophobic nanojars, functionalized with multiple alkyl chains, to transfer the carbonate ion from alkaline aqueous solutions to aliphatic solvents, and present the first liquid-liquid method for the extraction of carbonate.



Scheme 1. Pyrazole ligands used in the present study. Homoleptic nanojars can be obtained with pyrazoles shown in green; those in orange can only form heteroleptic nanojars, and the ones in red do not form nanojars under similar conditions.

2. RESULTS AND DISCUSSION

2.1. Synthesis of the new ligands. Pyrazole ligands substituted in the 4-position with mono-, di- or triethyleneglycol methyl ether chains are prepared in three steps (Scheme 2). First, the oligo(ethylene glycol) monomethyl ether (OEG), $\text{CH}_3(\text{OCH}_2\text{CH}_2)_z\text{OH}$ ($z = 1, 2$ or 3), is condensed with excess bromoacetaldehyde diethyl acetal in the presence of NaH, to yield the OEG diethyl acetals in quantitative yield. Next, the acetal is added to the Vilsmeier reagent obtained from POCl_3 and dimethylformamide, resulting in a mixture of OEG-substituted dimethylamino- and ethoxy-propenal, and smaller amounts of EtO-substituted dimethylamino- and ethoxy-propenal. This mixture is used without separation in the next step: treatment with hydrazine hydrate in methanol yields the corresponding OEG-substituted pyrazole, along with 4-ethoxypyrazole as side-product. The pure OEG-pyrazoles are obtained in 20–34% overall yields, based on the OEG starting material, after purification by column chromatography. 4-*n*-Octylpyrazole is synthesized similarly, using decanal diethyl acetal. 3,5-Dimethyl-4-*n*-octylpyrazole is prepared from hydrazine and 3-(*n*-octyl)pentane-2,4-dione, which in turn is obtained from acetylacetone and 1-iodooctane (Scheme 2).



Scheme 2. Synthesis of the novel OEG-pyrazole ligands, and new synthetic routes to 4-*n*-octylpyrazole and 3,5-dimethyl-4-*n*-octylpyrazole.

2.2. Synthesis of the nanojars. Nanojars of the general formula $[\text{CO}_3^{2-} \subset \{\text{Cu}(\text{OH})(\text{Rpz})\}_n]$ (pz = pyrazolate anion, R = substituent(s), $n = 27\text{--}31$) are synthesized using a one-pot reaction, by

stirring copper(II) nitrate, the pyrazole ligand (or a 1:1 mixture of two different pyrazole ligands) and a base (Cu:Rpz:OH in 1:1:2 molar ratio) in tetrahydrofuran for three days. Various hydroxides, such as MOH (M = Li⁺, Na⁺, K⁺, Rb⁺, Cs⁺, Bu₄N⁺, Et₄N⁺) and M(OH)₂ (M = Sr²⁺, Ba²⁺) can be employed as bases, along with the corresponding carbonates, which provide the incarcerated CO₃²⁻ ion. Alternatively, copper carbonate Cu₂CO₃(OH)₂ can be used both as copper- and carbonate-source, although it provides lower yields than the THF-soluble copper(II) nitrate.

Tetrabutylammonium was initially used as counterion in all cases, as it had been shown to promote crystallization.¹⁻³ In the case of highly hydrophobic nanojars based on pyrazoles with butyl or longer alkyl substituents, however, no ESI-MS signals can be detected when the counterion is Bu₄N⁺. The lack of ionization is attributed to extensive ion-pair formation, due to strong hydrophobic interactions between the long alkyl chains of the nanojars and the large Bu₄N⁺ counterions. Alkali metal counterions (Li⁺, Na⁺, K⁺, Rb⁺, Cs⁺) offer partial remedy for the problem, although in this case the MS signal is weakened by another factor: highly hydrophobic nanojars are insoluble in neat acetonitrile, therefore less polar tetrahydrofuran has to be added to the MS solvent in a 1:1 ratio to achieve solubility, which further suppresses the MS signal. Et₄N⁺ behaves similarly to Bu₄N⁺, although it does induce noteworthy changes in the crystal structure of the nanojar (see Crystallography section). Besides tetraalkylammonium and alkali or alkaline-earth metal cations, [K-18-crown-6]⁺ has also been successfully employed as counterion, which forms *in-situ* when 18-crown-6 is added to the reaction mixture. The identity of a particular counterion associated with the nanojar is confirmed by ESI-MS(+) (of the metal cations, only Rb⁺ and Cs⁺ have *m/z* values within the mass spectrometer's detection window).

The size distribution of the different [CO₃²⁻-{Cu(OH)(pz)}_n] nanojars (n = 27–31) varies slightly with the particular reaction conditions, such as the copper source, counterion and the base. In contrast, a much more pronounced variation is produced by the different substituents on the pyrazole ligands.

2.3. Effect of pyrazole substituents on nanojar structure. As seen in Figure 1, the pyrazole 4-positions point radially away from the nanojar. Therefore, no steric hindrance is predicted to be caused by substituents in the 4-position. Substitution at the pyrazole 3- and/or 5-positions, however, is expected to be more critical for nanojar formation, due to the all-*cis* configuration of the pyrazole ligands, which places substituents on the pyrazole units close to the neighboring

ligands. The steric hindrance is expected to be most significant for the two smaller side-rings, with pyrazole units pointing to the same side of the ring, while the larger, central ring can relieve the hindrance by orienting the pyrazole units alternately above and below the ring mean-plane (see also the Crystallography section).

All experiments discussed below are carried out in tetrahydrofuran as reaction medium, an excellent solvent for all nanojars, but not for the NaNO_3 by-product, which precipitates out of the reaction medium. The product mixtures are analyzed by ESI-MS in acetonitrile solutions, or, in the case of pyrazoles with butyl or longer chains, in a less polar $\text{CH}_3\text{CN}/\text{THF}$ (1:1) mixture. Mass spectra are shown in the Supporting Information (Figures S1–S30). Although the relative intensity of ESI-MS signals is dependent on individual ionization efficiencies, the various $[\text{CO}_3\text{C}\{\text{Cu}(\text{OH})(\text{pz})\}_n]^{2-}$ nanojars ($n = 27\text{--}31$) have identical charge and very similar size and shape, and are expected to have similar ionization efficiencies under identical ESI-MS conditions. Therefore, the observed ESI-MS signals should provide reliable information about the relative concentration of different nanojars based on the same ligand in a given solution. Indeed, this has been confirmed for nanojars based on the parent pyrazole ligand, using ^1H NMR spectroscopy.³ In the case of the mixed-pyrazole nanojars, however, ionization efficiencies drop drastically as the amount of the hydrophobic ligand component within a nanojar of a given size increases.

Formic acid is commonly used as an additive for mobile phases in reversed-phase liquid chromatography separations, as a buffer component, to improve peak shapes, and to promote ionization by producing $[\text{M}+\text{H}]^+$ ions. We find that nanojars are extremely sensitive to even traces of formic acid in the mass spectrometer; consequently, substituted nanojar species $[\text{CO}_3^{2-}\text{C}\{\text{Cu}_n(\text{OH})_n(\text{HCOO})_y(\text{pz})\}_{n-y}]$ ($y = 1\text{--}3$) are inevitably found in most spectra (at slightly lower m/z values than the pure nanojar), unless the instrument is opened up and thoroughly cleaned prior to injection of nanojar samples. In addition, adduct species are also observed occasionally, at larger m/z values than the pure nanojar.

2.3.1. Substitution of the pyrazole 4-position. Nanojars $[\text{CO}_3\text{C}\{\text{Cu}(\text{OH})(4\text{-Rpz})\}_n]^{2-}$ ($n = 27\text{--}31$) based on pyrazoles substituted in the 4-position with chains of varying lengths (up to 11 atoms) have been successfully prepared (Table 1, Figures S6–S13), indicating that linear chains do not interfere with nanojar formation, regardless of their length (Figure 1). In addition, nanojars with $\text{R} = \text{F}, \text{Cl}, \text{Br}, \text{I}, \text{phenyl}$ and CF_3 have been observed (Figures S2–S5, S14, S15), showing that

moderately bulky groups in the immediate vicinity of the pyrazole 4-position are also tolerated. In the case of 4-trifluoromethylpyrazole, a hexanuclear species $[\text{Cu}_6\text{O}_2(4\text{-CF}_3\text{pz})_9]^-$ (m/z 1629) is also formed beside the nanojars. Pyrazoles with potentially coordinating moieties ($\text{R} = \text{SO}_3\text{H}$, COOH , $\text{CH}=\text{O}$, OH) in the 4-position do not form nanojars: only insoluble, presumably polymeric products are obtained in those cases. With 4-nitropyrazole (LH), a soluble mixture of mono- to hexanuclear species (as indicated by the Cu-isotope pattern of the ESI-MS signals) is obtained (Figure S29). Within this mixture, $[\text{CuL}_2]^-$ (m/z 288), $[\text{Cu}_2\text{L}_4]^-$ (m/z 575), $[\text{NaCu}_3\text{OL}_3(\text{NO}_3)_2]^-$ (m/z 690), $[\text{Cu}_3\text{OL}_5]^-$ (m/z 767), $[\text{Cu}_4\text{O}_2\text{L}_6]^-$ (m/z 959), $[(\text{Bu}_4\text{N})\text{Cu}_3\text{OL}_6]^-$ (m/z 1122) and $[\text{Cu}_6\text{O}_2\text{L}_9]^-$ (m/z 1422) are identified as major components. The structure of related di-, tri-, tetra- and hexanuclear copper(II)-pyrazolate species has been established by X-ray diffraction.^{25–29} Partial reduction of Cu^{2+} to Cu^+ during ESI-MS is also common.³⁰

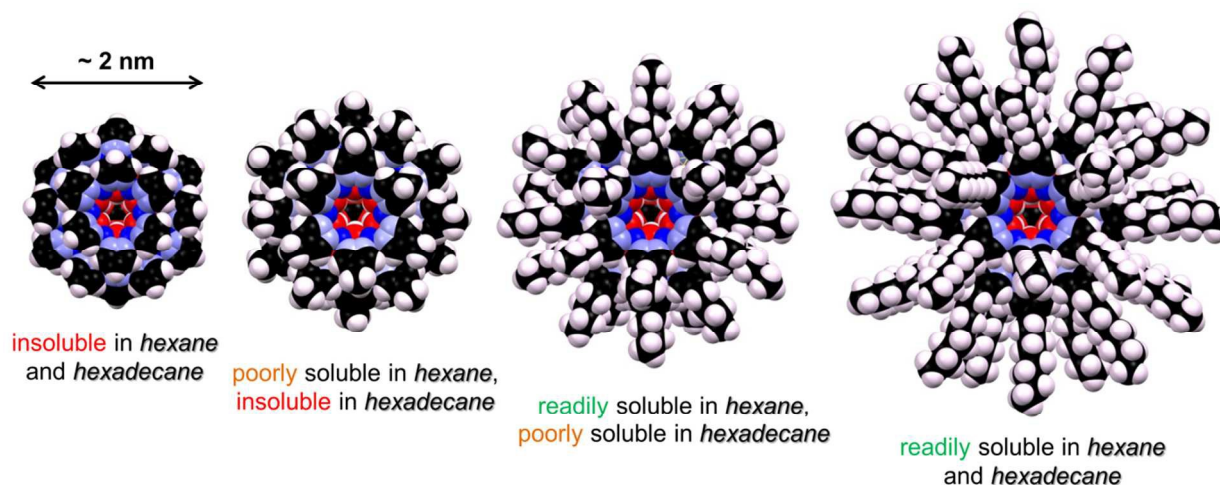


Figure 1. Space-filling models of $[\text{CO}_3\text{C}\{\text{Cu}(\text{OH})(4\text{-Rpz})\}_{27}]^{2-}$ nanojars (from left to right: $\text{R} = \text{H}$, Me , $n\text{Bu}$, $n\text{Oct}$).

2.3.2. Substitution of the pyrazole 3(5)-position. Alkyl substituents of various lengths (*e.g.*, methyl to *n*-octyl) are also tolerated at the pyrazole 3(5)-position (Table 1). It is likely that the longer alkyl chains turn away from the nanojar after the first CH_2 -unit connected to the pyrazole nucleus, thus avoiding interference from neighboring pyrazole units of the same Cu_x -ring. In contrast to 4-alkylpyrazoles, the Cu_{30} -nanojars $[\text{CO}_3\text{C}\{\text{Cu}(\text{OH})(3\text{-Rpz})\}_{30}]^{2-}$ are obtained almost exclusively with 3(5)-alkylpyrazoles (Figures S16–S20). No nanojars can be observed with bulky phenyl or CF_3 substituents at the pyrazole 3(5)-position, which yield only smaller, Cu_1 – Cu_6 species. However, a 1:1 molar mixture of 3(5)-PhpzH and HpzH affords an

approximately Gaussian distribution of nanojars $[\text{CO}_3\text{C}\{\text{Cu}_n(\text{OH})_n(3\text{-Phpz})_y(\text{pz})_{n-y}\}]^{2-}$ (Figure S23; major species: $n = 29$, $y \approx 5\text{--}19$). Similarly, a 1:1 mixture of 3(5)-F₃CpzH and HpzH produces a series of nanojars $[\text{CO}_3\text{C}\{\text{Cu}_n(\text{OH})_n(3(5)\text{-F}_3\text{Cpz})_y(\text{pz})_{n-y}\}]^{2-}$ (Figures S21, S22; major species: $n = 30$, $y \approx 6\text{--}17$), beside lower nuclearity species $[\text{Cu}(3\text{-CF}_3\text{pz})_2]^-$ (m/z 334), $[\text{Cu}_3\text{O}(\text{pz})(3\text{-CF}_3\text{pz})_4]^-$ (m/z 814), $[\text{Cu}_3\text{O}(3\text{-CF}_3\text{pz})_5]^-$ (m/z 882), $[\text{Cu}_4\text{O}(\text{pz})(3\text{-CF}_3\text{pz})_2(3\text{-CF}_3\text{pzH})_4]^-$ (m/z 1152), $[\text{Cu}_4\text{O}(3\text{-CF}_3\text{pz})_3(3\text{-CF}_3\text{pzH})_4]^-$ (m/z 1220). These latter two experiments demonstrate that some but not all pyrazole units of a nanojar can tolerate bulkier substituents in the 3(5)-position. As with 4-substituted pyrazoles, no nanojars are formed by pyrazoles with COOH, CH=O, NO₂, NH₂ or OH substituents at their 3(5)-position. In the case of 3-nitropyrazole (HL), a complex, soluble mixture of products (similar to the one obtained with 4-nitropyrazole), is characterized by ESI-MS (Figure S30): L^- (m/z 112), $[\text{CuL}_2]^-$ (m/z 288), $[\text{CuL}_3]^-$ (m/z 400), $[\text{Cu}_2\text{L}_3]^-$ (m/z 463), $[\text{Cu}_2\text{OL}_3]^-$ (m/z 479), $[\text{NaCuL}_4]^-$ (m/z 535), $[\text{Cu}_2(\text{OH})\text{L}_4]^-$ (m/z 592), $[\text{NaCu}_2\text{OL}_4]^-$ (m/z 614), $[\text{Cu}_3\text{O}(\text{OH})\text{L}_4]^-$ (m/z 672), $[\text{Cu}_2\text{L}_5]^-$ (m/z 687), $[\text{NaCu}_2(\text{OH})\text{L}_5]^-$ (m/z 727), $[\text{Cu}_3\text{OL}_5]^-$ (m/z 767), $[\text{NaCu}_2\text{L}_6]^-$ (m/z 822), $[\text{Cu}_4\text{O}_2\text{L}_5]^-$ (m/z 847), $[\text{NaCu}_3\text{OL}_6]^-$ (m/z 902), $[\text{Cu}_4\text{O}_2\text{L}_6]^-$ (m/z 959), $[(\text{Bu}_4\text{N})\text{Cu}_3\text{OL}_6]^-$ (m/z 1122), $[\text{Cu}_6\text{OL}_9]^-$ (m/z 1406), $[\text{Cu}_6\text{L}_{10}]^-$ (m/z 1502), $[\text{NaCu}_6\text{O}_2\text{L}_{10}(\text{NO}_3)]^-$ (m/z 1619).

2.3.3. Simultaneous substitution of the pyrazole 3- and 5-positions. As expected, no nanojars are obtained with 3,5-disubstituted pyrazoles as sole ligands, not even with the smallest methyl substituent. When used in a 1:1 molar mixture with HpzH, however, 3,5-dialkylpyrazoles and 3(5)methyl-5(3)trifluoromethylpyrazole do form mixed nanojars. The ESI-MS(−) spectrum of the nanojars $[\text{CO}_3\text{C}\{\text{Cu}_n(\text{OH})_n(3,5\text{-Me}_2\text{pz})_y(\text{pz})_{n-y}\}]^{2-}$, obtained from a 1:1 molar mixture of 3,5-Me₂pzH and HpzH, and Cu₂CO₃(OH)₂ as copper/carbonate source, shows three major groups of peaks ($n = 27$, $y \approx 0\text{--}9$; $n = 28$, $y \approx 6\text{--}13$; $n = 30$, $y \approx 10\text{--}14$) and small amounts of nanojars with $n = 29$, $y \approx 9\text{--}14$, and $n = 31$, $y \approx 10\text{--}14$ (Figure 2). When Cu(NO₃)₂ and Na₂CO₃ are used as copper and carbonate sources, respectively, a slightly different distribution is observed, with $n = 30$ as the major group, small amounts of $n = 28$, 29, and only traces of $n = 27$, 31 (Figure S24). Different ratios of 3,5-Me₂pzH and HpzH also lead to different distributions: a 2:1 molar mixture leads almost exclusively to $n = 30$, $y \approx 13\text{--}20$ (most abundant peak: $y = 14$), with small amounts of $n = 28$, $y \approx 12\text{--}18$, while a 5:1 ratio leads to $n = 30$, $y \approx 14\text{--}20$ (most abundant peak: $y = 20$). Using 3,5-Me₂pzH:HpzH ratios higher than 1:1 favors nanojars with larger value of y , but increasing amounts of low-nuclearity species are also produced at the same time. A 1:1 molar

mixture of 3,5-Me₂-4-ⁿOctpzH and HpzH also provides nanojars [CO₃C{Cu_n(OH)_n(3,5-Me₂-4-ⁿOctpz)_y(pz)_{n-y}}]²⁻, among which the ones with n = 30, y ≈ 10–16 constitute the major group. The ESI-MS(-) of [CO₃C{Cu_n(OH)_n(3,5-Et₂pz)_y(pz)_{n-y}}]²⁻ shows three major groups, n = 27, y ≈ 0–3; n = 29, y ≈ 0–10; n = 30, y ≈ 9–14, and small amounts of n = 31, y ≈ 0–11 and n = 32, y ≈ 12–15 (Figure S25). In the case of [CO₃C{Cu_n(OH)_n(3-ⁿBu-5-ⁿHexpz)_y(pz)_{n-y}}]²⁻, the major peaks correspond to the parent nanojars (n = 27, 29–31; y = 0), but smaller amounts of substituted species (y = 1–6) are also observed (Figure S26). In the case of a 3(5)-Me-5(3)-CF₃pzH:HpzH (1:1) mixture, the major species is [Cu₃O(pz)₃(3-Me-5-CF₃pz)₂]⁻ (m/z 706), along with other low-nuclearity species, and small amounts of nanojars are also observed: [CO₃C{Cu_n(OH)_n(3-Me-5-CF₃pz)_y(pz)_{n-y}}]²⁻ (n = 27, y ≈ 0–2; n = 29, y ≈ 0–2; n = 30, y ≈ 1–11) (Figures S27, S28). In the case of pyrazoles with bulkier substituents, such as bis(trifluoromethyl)-, di-^tbutyl- and diphenylpyrazole, however, not even mixed nanojars can be obtained. Di-^tbutyl- or diphenylpyrazole mixtures with HpzH (1:1) lead to [CO₃C{Cu(OH)(pz)}_n]²⁻ (n = 27–31) as the only THF-soluble products. In the case of 3,5-(CF₃)₂pzH:HpzH (1:1), the main species observed by ESI-MS(-) is the trinuclear [Cu₃O(pz)₃{3,5-(CF₃)₂pz}₂]⁻ (m/z 814), along with its adducts [Na_yCu₃O(pz)₃{3,5-(CF₃)₂pz}_{2+y}]⁻ (y = 1, m/z 1040; y = 2, m/z 1266; y = 3, m/z 1492; y = 4, m/z 1718; y = 5, m/z 1944) and [(Bu₄N)Cu₃O(pz)₃{(3,5-CF₃)₂pz}₃]⁻ (m/z 1260), as well as [Cu₃O(pz)₂{(3,5-CF₃)₂pz}₃]⁻ (m/z 950), [Cu₃OH(pz)₃{(3,5-CF₃)₂pz}₃]⁻ (m/z 1018) and its adduct [Na₂Cu₃OH(pz)₃{(3,5-CF₃)₂pz}₅]⁻ (m/z 1470). In addition, mononuclear [Cu{(3,5-CF₃)₂pz}₂]⁻ (m/z 470), tetranuclear [Na_yCu₄O(pz)₃{(3,5-CF₃)₂pz}_{3+y}]⁻ (y = 1, m/z 1307; y = 2, m/z 1533; y = 3, m/z 1759), hexanuclear [Na_yCu₆O₂(pz)₆{(3,5-CF₃)₂pz}_{3+y}]⁻ (y = 1, m/z 1651; y = 2, m/z 1877; y = 3, m/z 2103) as well as the free ligand and its Na-adducts, [Na_y{(3,5-CF₃)₂pz}_{1+y}]⁻ (y = 0, m/z 203; y = 1, m/z 429; y = 2, m/z 655), are also observed. Concurrently, the ESI-MS(+) spectrum of the same solution shows, beside the dominant Bu₄N⁺ ion, mostly trinuclear species [Na_yCu₃O(pz)₃{3,5-(CF₃)₂pz}_y]⁺ (y = 0, m/z 408; y = 1, m/z 634; y = 2, m/z 860; y = 3, m/z 1086; y = 4, m/z 1312; y = 5, m/z 1538), and smaller amounts of hexanuclear species [(Bu₄N)_yNa_zCu₆O₂(pz)₆{(3,5-CF₃)₂pz}_{1+y+z}]⁺ (y = 0, z = 3, m/z 1697; y = 0, z = 4, m/z 1923; y = 0, z = 5, m/z 2149; y = 2, z = 0, m/z 1910; y = 2, z = 1, m/z 2136; y = 2, z = 2, m/z 2362), [Na₃Cu₆O(OH)(pz)₆{(3,5-CF₃)₂pz}₅]⁺ (m/z 1901) and [(Bu₄N)₃Na₂Cu₆O₂(pz)₇{(3,5-CF₃)₂pz}₅]⁺ (m/z 2672). In general, we observe that the larger the substituents at the pyrazole 3/5 positions,

the less favorable the formation of the corresponding nanojars becomes, and the more low-nuclearity species are obtained.

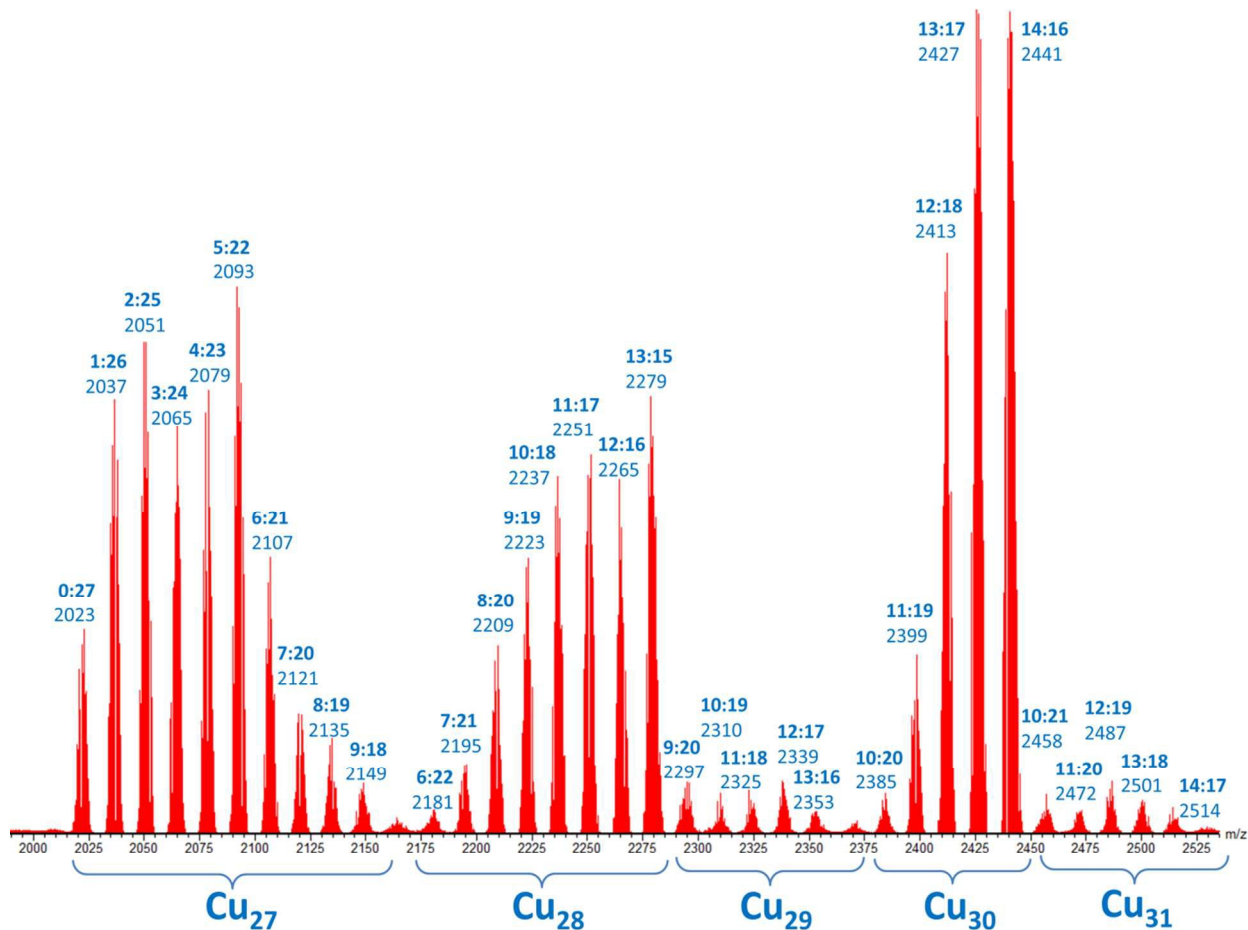


Figure 2. ESI-MS(-) spectrum of $[\text{CO}_3\text{C}\{\text{Cu}_n(\text{OH})_n(3,5\text{-Me}_2\text{pz})_y(\text{pz})_{n-y}\}]^{2-}$ ($y:n-y$ & m/z values shown) obtained from $\text{Cu}_2\text{CO}_3(\text{OH})_2$, 3,5-Me₂pzH/HpzH (1:1), NaOH and Bu₄NOH.

Table 1. [Nanojar]²⁻ species with differently substituted pyrazoles detected by ESI-MS(-). Occasionally, minor amounts of singly-charged [Counterion⁺(Nanojar²⁻)]⁻ species are also observed (not shown).

Entry	Pyrazole (LH)	Nanojar [CO ₃ ∩{Cu(OH)L _n }] ²⁻
1	HpzH	<i>m/z</i> 2023 (n = 27), 2171 (n = 29), 2244 (n = 30), 2318 (n = 31)
2	4-FpzH	<i>m/z</i> 2266 (n = 27), 2431 (n = 29), 2514 (n = 30), 2597 (n = 31)
3	4-ClpzH	<i>m/z</i> 2488 (n = 27), 2670 (n = 29), 2761 (n = 30), 2852 (n = 31)
4	4-BrpzH	<i>m/z</i> 3088 (n = 27), 3314 (n = 29), 3428 (n = 30), 3541 (n = 31)
5	4-IpzH	<i>m/z</i> 3723 (n = 27), 3996 (n = 29), 4133 (n = 30), 4270 (n = 31)
6	4-EtOpzH	<i>m/z</i> 2618 (n = 27), 2809 (n = 29), 3001 (n = 31)
7	4-MepzH	<i>m/z</i> 2212 (n = 27), 2374 (n = 29), 2455 (n = 30), 2536 (n = 31)
8	4- ⁿ BupzH	<i>m/z</i> 2780 (n = 27), 2984 (n = 29), 3188 (n = 31)
9	4- ⁿ OctpzH	<i>m/z</i> 3538 (n = 27), 3798 (n = 29), 4058 (n = 31)
10	4-(HOCH ₂ CH ₂ CH ₂)pzH	<i>m/z</i> 2807 (n = 27), 2910 (n = 28), 3013 (n = 29), 3116 (n = 30), 3218 (n = 31)
11	4-(CH ₃ OCH ₂ CH ₂ O)pzH	<i>m/z</i> 3023 (n = 27), 3245 (n = 29), 3466 (n = 31)
12	4-(CH ₃ (OCH ₂ CH ₂) ₂ O)pzH	<i>m/z</i> 3618 (n = 27), 3751 (n = 28), 3883 (n = 29), 4016 (n = 30), 4149 (n = 31)
12	4-(CH ₃ (OCH ₂ CH ₂) ₃ O)pzH	<i>m/z</i> 4212 (n = 27), 4522 (n = 29), 4832 (n = 31)
14	4-CF ₃ pzH	<i>m/z</i> 2941 (n = 27), 3157 (n = 29), 3372 (n = 31)
15	4-PhpzH	<i>m/z</i> 3050 (n = 27), 3274 (n = 29), 3386 (n = 30), 3498 (n = 31)
16	3-MepzH	<i>m/z</i> 2455 (n = 30)
17	3-EtpzH	<i>m/z</i> 2665 (n = 30)
18	3- ⁿ PrpzH	<i>m/z</i> 2876 (n = 30)
19	3- ⁿ BupzH	<i>m/z</i> 3086 (n = 30)
20	3- ⁿ OctpzH	<i>m/z</i> 3928 (n = 30)
21	3-CF ₃ pzH/HpzH (1:1)	[CO ₃ ∩{Cu _n (OH) _n (3-CF ₃ pz) _y (pz) _{n-y} }] ²⁻ (n = 27, 29, 30; y ≈ 3–17) <i>m/z</i> 2125–2822
22	3-PhpzH/HpzH (1:1)	[CO ₃ ∩{Cu _n (OH) _n (3-Phpz) _y (pz) _{n-y} }] ²⁻ (n = 27, 29; y ≈ 5–19) <i>m/z</i> 2251–2893
23	3,5-Me ₂ pzH/HpzH (1:1)	[CO ₃ ∩{Cu _n (OH) _n (3,5-Me ₂ pz) _y (pz) _{n-y} }] ²⁻ (n = 27–31, y ≈ 0–14) <i>m/z</i> 2023–2515
24	3,5-Me ₂ -4- ⁿ OctpzH/HpzH (1:1)	[CO ₃ ∩{Cu _n (OH) _n (3,5-Me ₂ -4- ⁿ Octpz) _y (pz) _{n-y} }] ²⁻ (n = 29–31, y ≈ 11–17) <i>m/z</i> 3015–3366
25	3,5-Et ₂ pzH/HpzH (1:1)	[CO ₃ ∩{Cu _n (OH) _n (3,5-Et ₂ pz) _y (pz) _{n-y} }] ²⁻ (n = 27–32, y ≈ 0–15) <i>m/z</i> 2023–2813
26	3- ⁿ Bu-5- ⁿ HexpzH/HpzH (1:1)	[CO ₃ ∩{Cu _n (OH) _n (3- ⁿ Bu-5- ⁿ Hexpz) _y (pz) _{n-y} }] ²⁻ (n = 27, 29–31, y ≈ 0–6) <i>m/z</i> 2023–2665
27	3-Me-5-CF ₃ pzH/HpzH (1:1)	[CO ₃ ∩{Cu _n (OH) _n (3-Me-5-CF ₃ pz) _y (pz) _{n-y} }] ²⁻ (n = 27, 29, 30, y ≈ 0–11) <i>m/z</i> 2023–2696

2.4. Crystallographic analysis. All three nanojar structures described herein consist of three neutral $[cis-Cu^{II}(\mu-OH)(\mu-pz)]_x$ rings, with a larger one ($x = 13$ or 14) sandwiched by two smaller ones ($x = 7, 8$ or 9), and they all incarcerate a carbonate ion in their central cavity. The central, larger ring is approximately flat, with the pyrazolate units symmetrically alternating slightly above and below the ring mean-plane, and they do not form hydrogen bonds to the carbonate ion. The smaller side-rings are bowl-shaped, with their pyrazolate moieties pointing away from the central ring, while their OH groups point toward the center of the nanojar and form multiple hydrogen bonds with the incarcerated CO_3^{2-} ion. While there is no direct bonding between the two smaller rings, they are both involved in multiple H-bonds and weak axial Cu–O interactions with the larger central ring. In the $[Cu(OH)(pz)]_x$ rings, Cu–O and Cu–N bond-lengths are within normal ranges (1.872(4)–1.967(4) and 1.923(4)–2.025(4) Å, respectively). Two Bu_4N^+ (or Et_4N^+) counterions balance the 2– charge of the carbonate ion in all nanojars.

2.4.1. $(Et_4N)_2[CO_3\{Cu(\mu-OH)(\mu-pz)\}_{29}(H_2O)_2]$ ($Et_4N-1 \cdot 2H_2O$). The nanojar in $Et_4N-1 \cdot 2H_2O$, which consists of three $[Cu(OH)(pz)]_x$ rings with $x = 8, 13$ and 8 , is similar to the one found in Bu_4N-1 (Figures S31–S33),³ however, the difference in counterion size (Et_4N^+ vs. Bu_4N^+) does induce significant changes in the molecular structure of the nanojar (Figure S34). Furthermore, despite a seemingly very similar overall crystal packing, the position of the nanojars relative to the crystal's symmetry elements is altered in Et_4N-1 compared to Bu_4N-1 . In Bu_4N-1 , the nanojar is located on a two-fold rotation axis (C_2), which runs through the C-atom of the incarcerated carbonate ion, symmetrically bisecting the latter. In Et_4N-1 , the nanojar is also located on a two-fold rotation axis, but unlike in Bu_4N-1 , the C_2 axis does not bisect the carbonate ion symmetrically, although it still runs through its central C-atom. As a result, the incarcerated carbonate ion in Et_4N-1 is disordered over two positions (50/50). Similarly to Bu_4N-1 ,³ in Et_4N-1 each Cu_8 -ring forms six H-bonds to the carbonate ion (for one Cu_8 -ring, $O \cdots O$: 2.81(1)–3.12(1) Å; average: 2.90(1) Å; for the other Cu_8 -ring, $O \cdots O$: 2.68(1)–3.01(1) Å; average: 2.90(1) Å). As in Bu_4N-1 , only eight of the twelve H-bonds to carbonate in Et_4N-1 have $O \cdots O$ distances <2.92(1) Å. The average H-bonding distance to carbonate is identical in Bu_4N-1 and Et_4N-1 (2.90(1) Å). The central Cu_{13} -ring forms five H-bonds to each Cu_8 -ring (average $O \cdots O$: 2.752(6) Å in Et_4N-1 , 2.766(6) Å in Bu_4N-1).

The presence of two water molecules (symmetry-related) in Et_4N-1 has significant consequences on the structure of the nanojar (no water is found in Bu_4N-1). Each H_2O molecule

is hydrogen-bonded to two OH groups across the Cu₈-ring (O19⋯O5: 2.851(6), O19⋯O2: 3.039(7) Å). As a result, those two OH groups are pulled closer to each other (O2⋯O5: 4.981(6) Å), compared to the corresponding distance in Bu₄N-1 (O⋯O: 5.596(6) Å), which lacks the bridging H₂O molecules. In fact, O2 and O5 are indeed the two most likely O-atoms to bind a bridging H₂O molecule, since those two O-atoms are not involved in significant H-bonding with the Cu₁₃-ring (O⋯O: 3.326(6) and 3.317(6) Å in Et₄N-1; 3.245(6) and 3.324(6) Å in Bu₄N-1). The distance between the two bonded Cu-atoms across the ring also decreases from 8.254(1) Å in Bu₄N-1 to 7.846(1) Å in Et₄N-1.

In both Et₄N-1 and Bu₄N-1, seven Cu-atoms of each Cu₈-ring form axial Cu–O interactions shorter than 3.00(5) Å with the Cu₁₃-ring (Et₄N-1, Cu⋯O: 2.367(5)–3.041(5) Å, average: 2.575(4) Å; Bu₄N-1, Cu⋯O: 2.340(4)–2.993(4) Å, average: 2.573(4) Å). The other Cu-atoms, including the ones of the Cu₁₃-ring, are at distances larger than 3.201(4) Å from the closest non-bonding O-atoms. Overall, there are fourteen Cu⋯O distances <3.00(5) Å in each nanojar, with an average of 2.574(4) Å.

2.4.2. (Bu₄N)₂[CO₃⊂{Cu₃₀(μ-OH)₃₀(μ-pz)₁₅(μ-3,5-Me₂pz)₁₅(H₂O)}] (Bu₄N-2). Within the triclinic (Pī) crystal lattice of **2**, the nanojar is located on a general position (with pseudo-mirror symmetry) and consists of three rings, [Cu(OH)(pz)]₇, [Cu(OH)(3,5-Me₂pz)]₁₄ and [Cu₉(OH)₉(pz)₈(3,5-Me₂pz)(H₂O)] (Figures 3, S35–S45). The encapsulated carbonate ion is found disordered over three positions (55/28/17), around the axis perpendicular to the central carbon atom (Figure S35). In each orientation, the carbonate ion is bound by twelve hydrogen bonds (average O⋯O: 2.90(2) Å), six each from the Cu₇- and Cu₉-rings, four to each of the three carbonate O-atoms. The Cu₇- and Cu₉-rings each accept seven H-bonds from the Cu₁₄-ring (Cu₇-ring, O⋯O: 2.787(5)–3.123(5) Å, average: 2.976(5) Å; Cu₉-ring, O⋯O: 2.750(5)–3.050(5) Å, average: 2.910(5) Å). Thus, the fourteen OH groups of the Cu₁₄-ring form alternating H-bonds with the Cu₇- and Cu₉-rings (average O⋯O: 2.943(5) Å). The presence of a water molecule within the nanojar is apparently the consequence of the steric hindrance caused by the methyl groups of the 3,5-Me₂pz unit within the Cu₉-ring. Thus, the H₂O molecule fills the void created between the Cu₉- and Cu₁₄-rings, as the Cu₂(μ-3,5-Me₂pz) moiety moves away from the two neighboring pyrazole units of the Cu₉-ring (Figure 3, bottom). This H₂O-molecule bridges the pair of Cu-atoms linked by the only 3,5-Me₂pz unit of the Cu₉-ring (Cu28⋯O31: 2.431(6), Cu29⋯O31: 2.450(7) Å), and donates a very short hydrogen bond to an adjacent OH-group of

the Cu₁₄-ring (O16–H160···O31: 2.482(9) Å). The overall H-bonding pattern in **2** is shown in Figure S44.

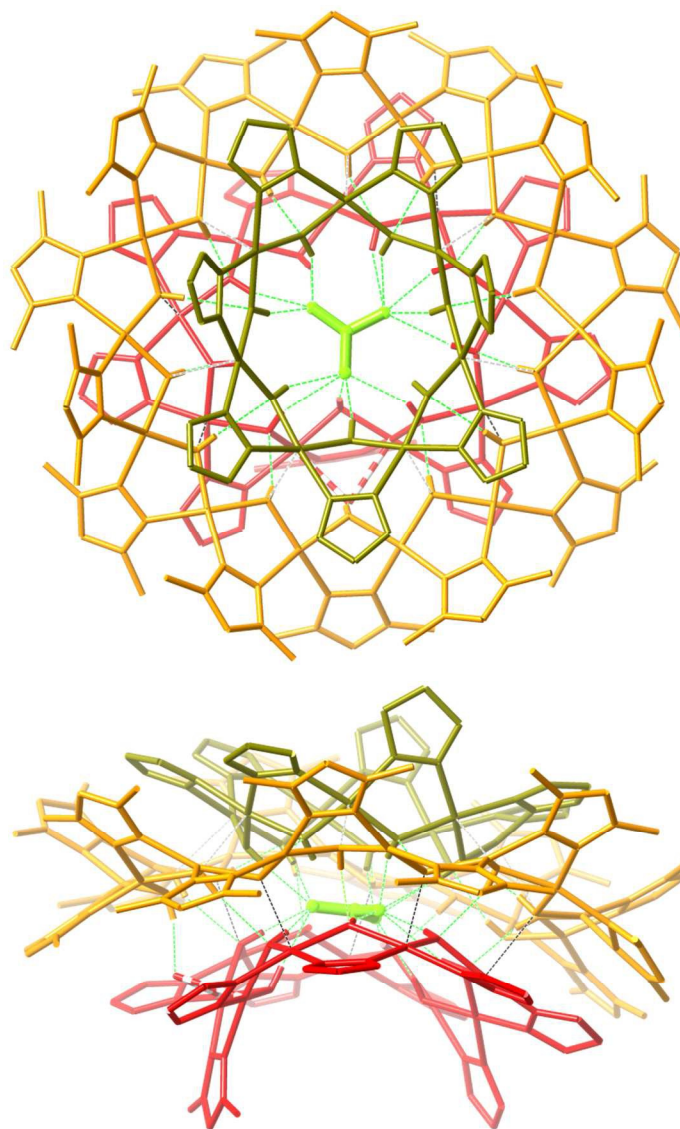


Figure 3. Top- and side-views of the crystal structure of **2**. Color scheme: Cu₇ – olive; Cu₉ – red; Cu₁₄ – orange; CO₃²⁻ – lime-green; H-bonds and weak Cu···O interactions – green and black dashed lines, respectively; Cu–O bonds to the coordinated H₂O molecule – red/white stripes. Only the major component of the disordered units, and no C–H and H₂O hydrogens, counterions or solvent molecules are shown.

The Cu₇- and Cu₉-rings form seven and six Cu···O contacts <3.000(1) Å, respectively, with O-atoms of the Cu₁₄-ring (Cu₇-ring, Cu···O: 2.516(4)–2.809(4) Å, average: 2.618(4) Å; Cu₉-ring, Cu···O: 2.407(4)–2.984(5) Å; average: 2.541(4) Å). Two Cu-atoms of the Cu₉-ring (bridged by the 3,5-Me₂pz ligand) bind the bridging H₂O molecule, which donates a H-bond to the Cu₁₄-ring. All other Cu-atoms, including the ones of the Cu₁₄-ring, are at distances larger

than 3.545(4) Å from the closest non-bonding O-atoms. Overall, there are thirteen Cu⋯O distances <3.000(1) Å in-between Cu_x-rings, with an average of 2.548(4) Å.

2.4.3. (Bu₄N)₂[CO₃⊂{Cu₃₀(μ-OH)₃₀(μ-pz)₁₆(μ-3,5-Me₂pz)₁₄}] (Bu₄N-3). Nanojar **3**, consisting of one [Cu(OH)(3,5-Me₂pz)]₁₄ and two [Cu(OH)(pz)]₈ rings, is located on a two-fold rotation axis (C₂), which runs perpendicular to the encapsulated carbonate ion, disordered accordingly over two positions (50/50). The position of the nanojar and encapsulated carbonate ion relative to the C₂ axis is clearly different than in Et₄N-**1** and Bu₄N-**1**, in which the C₂ axis is located in the plane of the carbonate ion. The central Cu₁₄-ring is made up by 3,5-dimethylpyrazolate ligands, while the two Cu₈ side rings contain only non-substituted pyrazole ligands.

The CO₃²⁻ ion is bound by a total of nine H-bonds in each disordered position (O⋯O: 2.63(9)–2.97(9) Å, average: 2.87(8) Å), four from one Cu₈-ring and five from the other, with each O-atom having three H-bonds. Each Cu₈-ring forms six H-bonds with the Cu₁₄-ring (O⋯O: 2.73(5)–2.96(5) Å, average: 2.87(5) Å). The two Cu₈-rings form six and eight Cu⋯O contacts <3.00(7) Å, respectively, with O-atoms of the Cu₁₄-ring (one Cu₈-ring, Cu⋯O: 2.52(3)–2.76(3) Å, average: 2.56(3) Å; other Cu₈-ring, Cu⋯O: 2.43(3)–3.10(3) Å; average: 2.67(3) Å). All other Cu-atoms, including the ones of the Cu₁₄-ring, are at distances larger than 3.13(3) Å from the closest non-bonding O-atoms. Overall, there are fourteen Cu⋯O distances <3.00(7) Å, with an average of 2.61(3) Å.

2.5. Solubilizing nanojars in hydrocarbon solvents and water. For liquid-liquid extraction purposes, solubility of the nanojar in long-chain aliphatic solvents is desirable. Characteristics of such solvents (typically C₉–C₁₈ alkanes/isoalkanes) include low toxicity, low vapor pressure, low flammability (high flash point), negligible solubility in water, chemical inertness, no odor or color, and low price. Nanojars comprised of the parent pyrazole ligand (HpzH), however, are insoluble in aliphatic solvents.¹ As illustrated in Figure 1, attachment of aliphatic chains of increasing lengths to the pyrazole 4-position leads to a gradual increase of the solubility of the corresponding nanojar in aliphatic solvents, such that nanojars based on 4-*n*-octylpyrazole are readily soluble in *n*-hexadecane (C₁₆, longest straight-chain alkane that is liquid at room temperature; mp = 18 °C) and even in heavy mineral oil (C₁₅–C₅₀). The same is true for the 3-*n*-octylpyrazole derivative, as well as the heteroleptic nanojars based on mixtures of non-substituted pyrazole and 3,5-dimethyl-4-*n*-octylpyrazole or 3-*n*-butyl-5-*n*-hexylpyrazole.

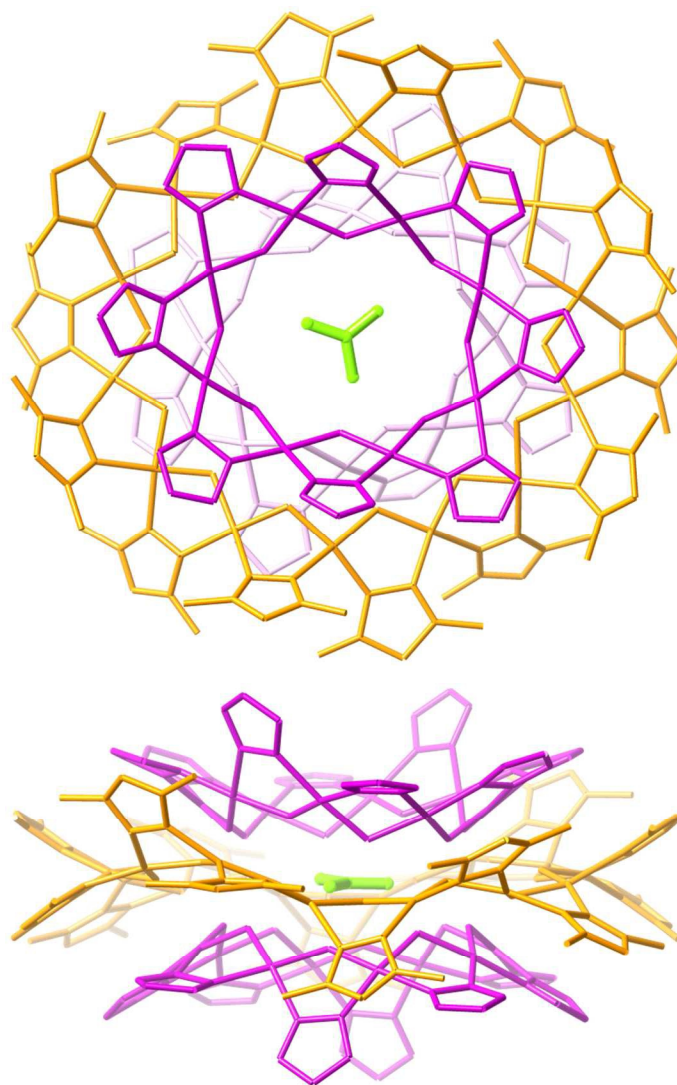


Figure 4. Top- and side-views of the crystal structure of **3**. Color scheme: Cu₈ – magenta; Cu₁₃ – orange; CO₃²⁻ – lime-green (only one position of the disordered carbonate, and no H-atoms, counterions or solvent molecules are shown).

Although all nanojars prepared so far are soluble in tetrahydrofuran, the solubility of the ones based on 4-halopyrazoles in toluene is drastically reduced compared to the parent nanojar and the alkyl- or ether-substituted ones. Thus, only the 4-fluoro-derivative is sparingly soluble in toluene, while the other halo-derivatives are practically insoluble. It is also noteworthy to mention that the solubility of the parent nanojar (but not of the ones with alkyl chain substituents) in toluene is lower when the counterion is a metal cation, compared to the Bu₄N⁺-salt.

Some future applications of nanojars might require solubility in water. Again, nanojars based on the parent non-substituted pyrazole are insoluble in water.¹ Polar, hydrophilic substituents, such as sulfonate, carboxylate or hydroxyl groups, would be expected to increase the solubility of the corresponding nanojars in water. However, those groups are also good donors (especially in their deprotonated forms), and, in the presence of Cu^{2+} , lead to the formation of polymeric products instead of nanojars.³¹⁻³³ To impart solubility in water while maintaining nanojar structure, we prepared novel pyrazole ligands with oligo(ethylene glycol) methyl ether chains attached to the 4-position, 4- $\text{CH}_3(\text{OCH}_2\text{CH}_2)_z\text{OpzH}$ ($z = 1-3$) (Scheme 2). While $\text{Na}_2[\text{CO}_3\text{C}\{\text{Cu}(\text{OH})(4\text{-CH}_3(\text{OCH}_2\text{CH}_2)_z\text{Opz})\}_n]$ ($n = 27-31$) nanojars are negligibly soluble in water when $z = 1$, the corresponding ones with $z = 2$ have noticeable solubility, and become readily soluble when $z = 3$.

2.6. Liquid-liquid extraction of carbonate from water. The carbonate ion (CO_3^{2-}) is in a pH-dependent equilibrium with the bicarbonate ion (HCO_3^-) and CO_2 .³⁴ At neutral pH, virtually no CO_3^{2-} ion is found in aqueous solution, while above pH~12, carbonate is found exclusively as CO_3^{2-} . Given its very large hydration energy ($\Delta G_h^\circ = -1315$ kJ/mol), the CO_3^{2-} ion is difficult to extract from water, compared to HCO_3^- ($\Delta G_h^\circ -368$ kJ/mol).²⁴ Herein we show that nanojars are excellent hosts for the solvent extraction of carbonate at pH 8–14. The industrial solvent Isopar-L is chosen as the organic extraction medium, which is a relatively harmless, colorless and odorless mixture of C_{11} – C_{13} isoalkanes, with low vapor pressure (0.3 mmHg at 20 °C, bp ~189–209 °C, compared to hexane: 132 mmHg, bp 69 °C). Carbonate is extracted quantitatively from a 1.0 mM aqueous Na_2CO_3 solution at pH 8–14 by stirring with a mixture of 4-R-pyrazole ($\text{R} = n\text{-butyl}$ or $n\text{-octyl}$), copper nitrate and NaOH (1:1:2 molar ratio) in Isopar-L, whereby nanojars $\text{Na}_2[\text{CO}_3\text{C}\{\text{Cu}(\text{OH})(4\text{-R-pz})\}_n]$, identified by ESI-MS(–), are separated into the organic phase. As the nanojar forms, it creates a highly hydrophilic cavity that encloses the carbonate ion, surrounded by a highly hydrophobic outer layer, which fully isolates the ion and provides solubility in the hydrophobic solvent. The incarcerated anion can be released as bicarbonate and/or CO_2 upon stripping the organic phase with a dilute nitric acid solution.

3. CONCLUSIONS

The present study, based on 40 differently substituted pyrazoles with one, two or three substituents of varying length, bulkiness and coordinating ability in the 3-, 4- and 5-positions,

provides a comprehensive picture of the effect of ligand substitution on nanojar structure. We find that reasonably bulky, non-coordinating substituents (such as alkyl chains, phenyl, CF_3) are tolerated at the pyrazole 4-position, while steric hindrance at the 3- and 5-positions will prevent the formation of nanojars. Although long, straight chains are also tolerated at the pyrazole 3(5)-position, no homoleptic nanojars can be obtained with 3-phenyl- or 3- CF_3 -pyrazole, nor with any 3,5-disubstituted pyrazoles, regardless of the size of the two substituents. In those cases, however, heteroleptic nanojars can be obtained in the presence of non-substituted pyrazole (or, presumably, 4-substituted pyrazoles), with the exception of 3,5- R_2 pyrazoles with bulky R groups (tBu , CF_3 , Ph), which are unable to fit within any nanojar. X-ray crystallographic studies on two of the various possible $(\text{Bu}_4\text{N})_2[\text{CO}_3\{\text{Cu}_{30}(\text{OH})_{30}(3,5\text{-Me}_2\text{pz})_y(\text{pz})_{30-y}\}]$ nanojars (with $y = 14$ and 15), obtained using a 1:1 mixture of 3,5-dimethylpyrazole and non-substituted pyrazole, demonstrate in both cases that the disubstituted ligands are preferentially incorporated into the larger, central $[\text{Cu}(\text{OH})(3,5\text{-Me}_2\text{pz})]_{14}$ ring (Cu_{14}). This approximately flat ring allows the ligands to symmetrically alternate above and below the ring mean-plane, thus avoiding steric hindrance between substituents on neighboring pyrazole units. In the nanojar with $y = 14$, the central Cu_{14} -ring is sandwiched in-between two smaller Cu_8 -rings, which are bowl-shaped and place the pyrazole ligands much closer to each other, leaving little room for substituents. In the case of the nanojar with $y = 15$, the two smaller rings are $[\text{Cu}(\text{OH})(\text{pz})]_7$ (Cu_7) and $[\text{Cu}_9(\text{OH})_9(3,5\text{-Me}_2\text{pz})(\text{pz})_8]$ (Cu_9). While the Cu_7 -ring is comprised only of non-substituted pyrazoles, the Cu_9 -ring does incorporate one disubstituted pyrazole. The crystal structure shows that this bulkier ligand turns sharply away from the neighboring pyrazole units of the Cu_9 -ring, to accommodate the substituents.

The limited ability of the smaller Cu_x -rings to incorporate disubstituted pyrazoles is also evident from the results of the ESI-MS studies. These studies show that even in the case of 3,5-dimethylpyrazole/pyrazole ratios larger than 14:16 (such as 15:15 or 20:10), the most abundant nanojar in the mixture is still $[\text{CO}_3\{\text{Cu}_{30}(\text{OH})_{30}(3,5\text{-Me}_2\text{pz})_{14}(\text{pz})_{16}\}]^{2-}$, in which the central ring is fully substituted, and the two smaller side-rings are not substituted at all. Not only is the nanojar with $y = 14$ the most abundant species in these mixtures, but there is also an abrupt drop in the abundance of the nanojars with $y > 14$, reflecting the weaker tendency of the smaller Cu_x -rings to incorporate disubstituted pyrazoles. Nevertheless, homoleptic Cu_{30} -nanojars based solely on 3-substituted pyrazoles can be obtained, in which case the monosubstituted ligands of the

smaller Cu_x-rings are likely found in a propeller-type arrangement, minimizing the repulsion between substituents and neighboring pyrazole units. Regardless of the position on the pyrazole ligand, COOH, SO₃H, CH=O, OH, NH₂ and NO₂ groups prevent the formation of nanojars, and either insoluble, presumably polymeric, or soluble, small complexes (Cu₁–Cu₆, in the case of 3- and 4-nitropyrazole) are obtained instead. This study also led to new synthesis methods of 4-*n*-octylpyrazole, 3,5-dimethyl-4-*n*-octylpyrazole and 4-ethoxypyrazole, and inspired the preparation of novel pyrazole ligands with oligoether chain substituents, which render nanojars soluble in water.

We have demonstrated that the solubility of nanojars in various solvents can be conveniently tuned by varying the substitution of the pyrazole ligands. Thus, alkyl chains of increasing lengths impart increasing solubility in aliphatic solvents, rendering nanojars amenable for the large-scale liquid-liquid extraction of anions with large hydration energies from aqueous solutions. The extraction process is exemplified here by the efficient transfer of carbonate from water to an aliphatic solvent, which is unprecedented for an anion with such large hydration energy. We are currently exploring the removal of toxic anions, such as arsenate, chromate and selenate, from water using nanojars as extracting agents.

4. EXPERIMENTAL SECTION

4.1. Materials and methods. 4-Hydroxypyrazole,³⁵ 3-hydroxypyrazole,³⁶ 4-fluoropyrazole,³⁷ 4-chloropyrazole,³⁸ 4-bromopyrazole,³⁸ 4-iodopyrazole,²⁹ 4-nitropyrazole,³⁹ 4-formylpyrazole,⁴⁰ 3-formylpyrazole,⁴¹ pyrazole-4-sulfonic acid,⁴² 3,5-diethylpyrazole,⁴³ 3(5)-*n*-butyl-5(3)-*n*-hexylpzH,⁴⁴ 3,5-di-*tert*-butylpyrazole,⁴⁵ 3,5-bis(trifluoromethyl)pyrazole,⁴⁶ 3,5-diphenylpyrazole,⁴⁷ 4-phenylpyrazole,⁴⁸ 4-*n*-butylpyrazole,⁴⁹ 4-(3-hydroxypropyl)pyrazole⁵⁰ and 3(5)-*n*-alkylpyrazoles⁵¹ (alkyl = Me, Et, Pr, Bu, Oct) are prepared according to published procedures. All other commercially available chemicals are used as received. Reactions are carried out in the air, unless stated otherwise. Hexane (mixture of isomers) and dimethylformamide are dried with molecular sieves.

Mass spectrometric analysis of the nanojars is performed on a Waters Synapt G1 HDMS instrument, using an electrospray ionization source. 10⁻⁴–10⁻⁵ M sample solutions are prepared in CH₃CN, except for the nanojars with butyl or longer alkyl chain substituents, in which case a 1:1 (vol.) mixture of CH₃CN/THF is used. Samples are infused by a syringe pump at 5 μL/min

and nitrogen is supplied as nebulizing gas at 500 L/h. The electrospray capillary voltage is set to -2.5 or $+3.0$ kV, respectively, with a desolvation temperature of 110 °C. The sampling and extraction cones are maintained at 40 V (100 V for nanojars with long alkyl chain substituents) and 4.0 V, respectively, at 80 °C.

4.2. Decanal diethyl acetal. Decanal (47.1 mL, 39.1 g, 250 mmol), triethyl orthoformate (41.6 mL, 37.1 g, 250 mmol) and *p*-toluenesulfonic acid monohydrate (476 mg, 2.50 mmol) are dissolved in 250 mL absolute ethanol. After standing for 1 hour at room temperature, ^1H NMR indicates that the reaction is practically complete. The solution is left to stand overnight, then it is poured into 500 mL of saturated sodium bicarbonate solution (~ 96 g $\text{NaHCO}_3/\text{L H}_2\text{O}$ at 20 °C), and is extracted with ethyl acetate (5×100 mL). The combined organic extracts are dried overnight with anhydrous Na_2SO_4 , followed by evaporation of the solvent and drying under high vacuum to yield 56.4 g (98%) of decanal diethyl acetal. ^1H NMR (400 MHz, CDCl_3): δ 4.46 (t, 1H , $^3J = 6$ Hz), 3.62 (dq, 2H , $^3J = 7$ Hz), 3.47 (dq, 2H , $^3J = 7$ Hz), 1.58 (m, 2H), 1.25 (m, 14H), 1.19 (t, 6H , $^3J = 7$ Hz), 0.86 (t, 3H , $^3J = 7$ Hz) ppm.

4.3. General method of preparation for 7-ethoxy-2,5,8-trioxadecane, 10-ethoxy-2,5,8,11-tetraoxatridecane and 13-ethoxy-2,5,8,11,14-pentaoxahexadecane. NaH (60% dispersion in mineral oil, 4.000 g, 100 mmol) is placed in a 250 mL three-neck, round-bottom flask, which is connected to a Schlenk line. A condenser is attached, the third neck is sealed with a rubber septum, and the system is evacuated and purged with nitrogen three times. The mineral oil is washed away from the sodium hydride by rinsing with anhydrous hexane. The hexane (50 mL) is introduced with an N_2 -purged syringe, and the mixture is stirred for 3 minutes. After the NaH has settled, the supernatant is removed with a syringe, and the procedure is repeated three more times. The residue is then dried thoroughly by applying high vacuum. Neat bromoacetaldehyde diethyl acetal (100 mL, 131 g, 0.664 mol) is added by syringe under stirring, followed by the dropwise addition of the oligo(ethylene glycol) monomethyl ether, $\text{CH}_3(\text{OCH}_2\text{CH}_2)_z\text{OH}$ (50.00 mmole; $z = 1$, 3.950 mL, 3.8045 g; $z = 2$, 5.800 mL, 6.007 g; $z = 3$, 8.000 mL, 8.210 g). The reaction is exothermic and is accompanied by a color change from light grey to brown. After heating to 100 °C for 48 hours under stirring, the reaction mixture is left to cool down to room temperature. Water (20 mL) is added to quench the unreacted NaH, and the excess bromoacetaldehyde diethyl acetal is distilled off under high vacuum at ~ 30 °C. The dark brown viscous residue is taken up into dichloromethane (200 mL) and is washed with water (40 mL)

twice, followed by drying the organic layer with MgSO₄ overnight. After filtration, the solvent is removed under vacuum at ~ 30 °C and the product is obtained as red-brown viscous oil in close to quantitative yield. Although the product is of sufficient purity to be used in the next step, vacuum distillation can be employed if further purification is needed.

4.3.1. 7-Ethoxy-2,5,8-trioxadecane. Obtained as colorless oil after distillation (b.p. 47–49 °C at 0.005 mmHg). ¹H NMR (400 MHz, CDCl₃): δ 4.63 (t, 1H, ³J = 5 Hz, CH(OCH₃CH₂)₂), 3.65–3.68 (m, 4H, OCH₂CH₃), 3.52–3.59 (m, 6H, OCH₂CH₂ and OCH₂CH), 3.36 (s, 3H, OCH₃), 1.20 (t, 6H, OCH₂CH₃) ppm. ¹³C NMR (101 MHz, CDCl₃): δ 101.3, 72.03, 70.9, 70.96, 62.4, 59.1 ppm. HRMS (ESI-TOF) *m/z*: [M+Na]⁺ calcd for C₉H₂₀NaO₄ 215.1259; found 215.1254.

4.3.2. 10-Ethoxy-2,5,8,11-tetraoxatridecane. Obtained as colorless oil after distillation (b.p. 72–73 °C at 0.005 mmHg). ¹H NMR (400MHz, CDCl₃): δ 4.67 (t, 1H, CH(OCH₃CH₂)₂), 3.50–3.79 (m, 14H, OCH₂ and OCH₂CH₃), 3.35 (s, 3H, OCH₃), 1.19 (t, 3H, CH₂CH₃) ppm. ¹³C NMR (101 MHz, CDCl₃): δ 101.4, 72.0, 71.7, 70.9, 70.7, 70.6, 65.7, 62.5, 59.2, 15.4 ppm. HRMS (ESI-TOF) *m/z*: [M+Na]⁺ calcd for C₁₁H₂₄NaO₅ 259.1521; found 259.1514.

4.3.3. 13-Ethoxy-2,5,8,11,14-pentaoxahexadecane. Obtained as brown viscous oil. ¹H NMR (400 MHz, CDCl₃): δ 4.62 (t, 1H, ³J = 6 Hz, CH(OCH₃CH₂)₂), 3.62–3.66 (m, 12H, CH₂CH₃ and OCH₂CH₂), 3.51–3.59 (m, 6H, OCH₂CH₂), 3.36 (s, 3H, OCH₃), 1.20 (t, 6H, CH₂CH₃) ppm. ¹³C NMR (101 MHz, CDCl₃): δ 101.3, 72.012, 71.967, 70.965, 70.705, 70.667, 70.664, 70.613, 62.4, 59.1 ppm.

4.4. General method of preparation for 3-R-2-octyl-prop-2-enal, 3-R-2-(2-methoxyethoxy)-prop-2-enal, 3-R-2-(2-(2-methoxyethoxy)ethoxy)-prop-2-enal and 3-R-2(2-(2-(2-methoxyethoxy)ethoxy)ethoxy)-prop-2-enal (R = NMe₂ and OEt).

POCl₃ (6.38 ml, 10.5 g, 68.4 mmol) is added to a 100 mL Schlenk-flask equipped with a pressure-equalizing addition funnel, sealed with a rubber septum. The system is evacuated and purged with nitrogen a few times while cooling in an ice bath. DMF (5.86 ml, 5.53 g, 75.7 mmol) is injected into the additional funnel via N₂-purged syringe, and is added dropwise to POCl₃ under stirring. Decanal diethyl acetal (7.26 g, 31.5 mmol) or CH₃(OCH₂CH₂)_zOCH₂CH(OEt)₂ (31.5 mmol; z = 1, 6.05 g; z = 2, 7.43 g; z = 3, 8.82 g) is added via syringe to the colorless crystalline Vilsmeier reagent obtained. The ice bath is replaced with a water bath and the reaction mixture is allowed to warm up to room temperature. The color of the reaction slowly turns yellow. The temperature of the water bath is raised to 70–75 °C, causing

the color to quickly turn dark orange and then dark red. A vigorous reaction ensues, accompanied by a large increase in pressure (relieved through the Schlenk line's oil bubbler). The reaction mixture is kept at the same temperature for 2 hours, then the dark brown-red, viscous solution is poured into 50 g crushed ice and is left to stand overnight. Next day, the mixture is extracted with CH_2Cl_2 (2×25 mL), followed by Et_2O (25 mL). The aqueous phase is neutralized with solid K_2CO_3 (20 g), which is added in small portions, under stirring, until $\text{pH} \approx 8$. The orange-red solution is extracted again with CH_2Cl_2 (5×25 mL) and Et_2O (2×20 mL). The combined organic extracts are dried overnight with anhydrous MgSO_4 . After filtration, the solvent is evaporated under vacuum and DMF is distilled off in vacuum on a water bath at 80°C . The resulting dark red-brown oil consists of a mixture of 3-(dimethylamino)-2-*n*-octyl-prop-2-enal and 3-ethoxy-2-*n*-octyl-prop-2-enal in the case of $\text{CH}_3(\text{CH}_2)_8\text{CH}(\text{OEt})_2$, and OEG-substituted dimethylamino- and ethoxy-propenal, as well as smaller amounts of EtO-substituted dimethylamino- and ethoxy-propenal in the case of $\text{CH}_3(\text{OCH}_2\text{CH}_2)_z\text{OCH}_2\text{CH}(\text{OEt})_2$. These mixtures are used without separation in the next step.

4.5. General method of preparation for 4-octylpyrazole, 4-(2-methoxyethoxy)pyrazole, 4-(2-(2-methoxyethoxy)ethoxy)pyrazole and 4-(2-(2-(2-methoxyethoxy)ethoxy)ethoxy)pyrazole.

The mixtures obtained above are dissolved in methanol (60 mL), hydrazine monohydrate (1.95 ml, 1.98 g, 39.5 mmol) is added and the mixture is refluxed for 2 hours. After cooling to room temperature, the solvent is removed under vacuum. The dark red-brown oil is subjected to purification by vacuum distillation or column chromatography.

4.5.1. *4-Octylpyrazole*. Vacuum distillation using a Vigreux column provides pure 4-octylpyrazole as a colorless liquid (b.p. 143°C at ~ 0.1 mmHg), which solidifies on cooling. Yield: 4.21 g (75% based on decanal). ^1H NMR (400 MHz, CDCl_3): δ 12.07 (s, br, 1H), 7.40 (s, 2H), 2.49 (t, 2H, $^3J = 8$ Hz), 1.56 (m, 2H), 1.30 (m, 10H), 0.90 (t, 3H, $^3J = 7$ Hz) ppm. ^{13}C NMR (101 MHz, CDCl_3): δ 132.5, 121.2, 32.0, 31.2, 29.6, 29.4, 24.2, 22.8, 14.2 ppm.

4.5.2. *4-(2-methoxyethoxy)pyrazole*. Purified by column chromatography on silica gel (300 g) using neat ethyl acetate as eluent (R_f 0.49). The product (1.52 g) is obtained as an orange oil in 34% overall yield (based on ethylene glycol monomethyl ether). ^1H NMR (400MHz, CDCl_3): δ 7.29 (s, 2H, 3,5-*H*-pz), 4.01–4.03 (m, 2H, OCH_2), 3.67–3.70 (m, 2H, OCH_2), 3.42 (s, 3H, OCH_3) ppm. ^{13}C NMR (101 MHz, CDCl_3): δ 145.5, 121.1, 71.1, 59.2 ppm. HRMS (ESI-TOF) m/z : $[\text{M}+\text{Na}]^+$ calcd for $\text{C}_6\text{H}_{10}\text{N}_2\text{NaO}_2$ 165.0640; found 165.0643.

4.5.3. *4-(2-(2-methoxyethoxy)ethoxy)pyrazole*. Purified by column chromatography on silica gel (300 g) using neat ethyl acetate as eluent (R_f 0.35). The product (1.50 g) is obtained as an orange-red oil in 26% overall yield (based on diethylene glycol monomethyl ether). ^1H NMR (400 MHz, CDCl_3): δ 7.28 (s, 2H, 3,5-*H*-pz), 4.02 (t, 2H, OCH_2 , $^3J = 4$ Hz), 3.78 (t, 2H, OCH_2 , $^3J = 4$ Hz), 3.68 (t, 2H, OCH_2 , $^3J = 4$ Hz), 3.56 (t, 2H, OCH_2 , $^3J = 4$ Hz), 3.37 (s, 3H, OCH_3) ppm. ^{13}C NMR (101 MHz, CDCl_3): δ 145.5, 120.9, 71.9, 71.2, 70.7, 69.9, 59.1 ppm. HRMS (ESI-TOF) m/z : $[\text{M}+\text{Na}]^+$ calcd for $\text{C}_8\text{H}_{14}\text{N}_2\text{NaO}_3$ 209.09021; found 209.0902.

4.5.4. *4-(2-(2-(2-methoxyethoxy)ethoxy)ethoxy)pyrazole*. Purified by column chromatography on silica gel (300 g) using an eluent gradient as follows: 95:5 EtOAc:hexanes first, neat EtOAc second, 95:5 EtOAc:MeOH third, and 90:10 EtOAc:MeOH last. The product (1.44 g) is obtained as an orange-yellow oil in 20% overall yield (based on triethylene glycol monomethyl ether). ^1H NMR (400 MHz, CDCl_3): δ 7.28 (s, 2H, 3(5)-*H*-pz), 4.00–4.02 (m, 2H, OCH_2), 3.76–3.79 (m, 2H, OCH_2), 3.62–3.71 (m, 6H, $\text{CH}_2\text{OCH}_2\text{CH}_2$), 3.53–3.55 (m, 2H, OCH_2), 3.36 (s, 3H, OCH_3). ^{13}C NMR (100 MHz, CDCl_3): δ 145.5, 121.0, 71.9, 71.3, 70.7, 70.6, 70.5, 69.9, 59.1 ppm. HRMS (ESI-TOF) m/z : $[\text{M}+\text{Na}]^+$ calcd for $\text{C}_{10}\text{H}_{18}\text{N}_2\text{NaO}_4$ 253.1164; found 253.1173.

4.6. 4-Ethoxypyrazole. Obtained as a side-product during the column chromatography of the mono-, di- and triethyleneglycol methyl ether-substituted pyrazoles described above, in 5:8, 5:10 and 5:7 molar ratios, respectively (4-EtOpyrazole:4-OEGpyrazole). ^1H NMR (400 MHz, CDCl_3): δ 7.28 (s, 2H, 3,5-*H*-pz), 3.94 (q, 2H, $^3J = 7$ Hz, CH_2CH_3), 1.37 (t, 3H, $^3J = 7$ Hz, CH_2CH_3). ^{13}C NMR (101 MHz, CDCl_3): δ 145.6, 120.8, 67.5, 15.0 ppm. HRMS (ESI-TOF) m/z : $[\text{M}+\text{H}]^+$ calcd for $\text{C}_5\text{H}_9\text{N}_2\text{O}$ 113.0715; found 113.0695.

4.7. 3,5-Dimethyl-4-octylpyrazole. First, 3-(*n*-octyl)pentane-2,4-dione is prepared as follows. A mixture of acetylacetone (30.0 ml, 29.2 g, 0.292 mol) and 1-iodooctane (53.0 ml, 70.5 g, 0.293 mol) was added dropwise to a stirred suspension of anhydrous K_2CO_3 (50.0 g, 0.362 mol) in 50 mL acetonitrile. The reaction mixture was refluxed overnight with stirring. After cooling to room temperature, the solid was filtered off and washed with acetone. The organic solvents were evaporated on a rotavap, water was added to the residue and it was extracted with diethyl ether. After evaporation of the ether, the residue (60.7 g) was fractionally distilled under vacuum using a Vigreux column, and the fraction distilling at 104 °C (43.5 g) was redistilled. The fraction distilling at 117 °C (41.0 g, yield: ~66%) was found to be a mixture of the keto and enol forms of

3-(*n*-octyl)pentane-2,4-dione, with a small amount of O-alkylated enol. This mixture was used in the next step without further purification.

Hydrazine hydrate (N₂H₄ 50–60% in H₂O, 12.414 g) is added dropwise to a solution of 3-(*n*-octyl)pentane-2,4-dione (38.851 g) in 150 mL EtOH with stirring. The mixture is refluxed for 14 hours and the solvent is evaporated on a rotavap. The residue (38.664 g) is fractionally distilled under vacuum, using a Vigreux column. The fraction distilling at 155–160 °C (32.721 g) is redistilled, yielding 32.125 g (56% based on acetylacetone) of pure 3,5-dimethyl-4-*n*-octylpyrazole boiling at 160 °C. ¹H NMR (400 MHz, CDCl₃): 2.31 (t, 2H, ³J = 8 Hz), 2.19 (s, 6H), 1.41 (m, 2H), 1.27 (m, 10H), 0.87 (t, 3H, ³J = 7 Hz) ppm. ¹³C NMR (101 MHz, CDCl₃): 142.0, 115.8, 32.0, 30.8, 29.6, 29.5, 29.4, 23.1, 22.8, 14.2, 11.0.

4.8. General methods of preparation for nanojars. In each case, the identity of the resulting nanojar mixtures is determined using ESI-MS (Table 1).

Method A. Cu(NO₃)₂·2.5H₂O (1.000 g, 4.30 mmol), pyrazole ligand (4.30 mmol), NaOH (332 mg, 8.30 mmol), Na₂CO₃·H₂O (533 mg, 4.30 mmol) and Bu₄NOH (1M in H₂O, 318 mg, 0.318 mmol) are stirred in THF (20 mL) for 3 days. After filtration, the deep blue solution is left to evaporate. The dark blue residue is stirred with THF (15 mL), then filtered and slowly added to deionized water (100 ml) under stirring. The blue precipitate is filtered, washed with water and dried in vacuum to yield (Bu₄N)₂[CO₃⊂{Cu(OH)(pz)}_n] (n = 27–31). In the case of mixed-pyrazole nanojars, 2.15 mmol of each pyrazole ligand is employed. Et₄NOH can also be used instead of Bu₄NOH.

Method B. Same as above, except that Cu(NO₃)₂·2.5H₂O and Na₂CO₃·H₂O are replaced by CuCO₃·Cu(OH)₂ (475 mg, 2.15 mmol).

Method C. Same as method A, except that M^IOH (8.60 mmol; M^I = Li⁺, Na⁺, K⁺, Rb⁺, Cs⁺) or M^{II}(OH)₂·8H₂O (4.30 mmol; M^{II} = Sr²⁺, Ba²⁺) are used as base and counterion-source instead of NaOH/Bu₄NOH. The corresponding metal carbonate is employed as carbonate-source. Depending on the base used, M^I₂[CO₃⊂{Cu(OH)(pz)}_n] or M^{II}[CO₃⊂{Cu(OH)(pz)}_n] (n = 27–31) nanojars are obtained. In the case of KOH, 18-crown-6 (137 mg, 0.518 mmol) can be added to the reaction mixture to obtain (K⁺⊂18-crown-6)₂[CO₃²⁻⊂{Cu(OH)(pz)}_n] (n = 27–31).

4.9. Liquid-liquid extraction of carbonate from water. To a 1.0 mM aqueous solution of Na₂CO₃ at pH 8–14 (7.9 mg anhydrous Na₂CO₃ in 75 mL NaOH 10⁻⁶–1 M) is added Cu(NO₃)₂·2.5H₂O (500 mg, 2.15 mmol), 4-R-pyrazole (R = *n*-butyl, 267 mg, 2.15 mmol; R = *n*-

octyl, 385 mg, 2.15 mmol), NaOH (172 mg, 4.30 mmol) and ISOPAR-L (75 mL), and the mixture is stirred vigorously under N₂. The organic phase immediately starts turning blue, and the aqueous phase gradually turns colorless. ESI-MS of the deep-blue organic phase indicates the presence of [CO₃C{Cu(OH)(4-R-pz)}_n]²⁻, at *m/z* 2780 (Cu₂₇), 2984 (Cu₂₉), 3188 (Cu₃₁) (R = *n*-butyl), and *m/z* 3538 (Cu₂₇), 3798 (Cu₂₉), 4058 (Cu₃₁) (R = *n*-octyl), respectively.

4.10. X-ray crystallography. Single crystals are grown by hexane vapor diffusion to a toluene solution of the nanojars. Once removed from the mother liquor, the crystals are extremely sensitive to solvent loss at ambient conditions and are mounted quickly under a cryostream (100 K) to prevent decomposition. X-ray diffraction data are collected at 100 K from a single-crystal mounted atop a glass fiber under Paratone-N oil, with a Bruker SMART APEX II diffractometer using graphite-monochromated Mo-K α ($\lambda = 0.71073 \text{ \AA}$) radiation. The structures are solved by employing SHELXTL direct methods and refined by full-matrix least squares on F^2 , using the APEX2 v2014.9-0 software package.⁵² All non-H atoms are refined with independent anisotropic displacement parameters, except the disordered molecules. C–H hydrogen atoms are placed in idealized positions and refined using the riding model. O–H hydrogen atoms are located from the difference Fourier maps; their displacement parameters are fixed to be 20 % larger than those of the attached O atoms. For the disordered molecules, geometrical restraints are used and H-atoms are not assigned. Crystallographic details are summarized in Table 2, and thermal ellipsoid plots, as well as structural details, are shown in the Supporting Information. Crystallographic data have been deposited at the Cambridge Crystallographic Data Centre (deposition numbers: CCDC 1455325 and 1455326). Copies of the data can be obtained free of charge via <http://www.ccdc.cam.ac.uk/conts/retrieving.html> (or from the Cambridge Crystallographic Data Centre, 12, Union Road, Cambridge, CB2 1EZ, UK; fax: +44 1223 336033; e-mail: deposit@ccdc.cam.ac.uk).

(Et₄N)₂[CO₃²⁻C{*cis*-Cu^{II}(μ -OH)(μ -pz)}₈₊₁₃₊₈](C₇H₈)₄(H₂O)₂: Et₄N-**1**(C₇H₈)₄(H₂O)₂. One Cu(OH)(pz)Cu unit of the Cu₁₃-ring is disordered (50/50) about the two-fold rotation symmetry axis running through the nanojar. The toluene solvent molecules are disordered over two positions (50/50); one of them is disordered about the C₂ rotation axis.

(Bu₄N)₂[CO₃²⁻C{*cis*-Cu^{II}(μ -OH)(μ -pz)}₇{*cis*-Cu^{II}(μ -OH)(μ -3,5-Me₂pz)}₁₄{*cis*-Cu^{II}(μ -OH)₉(μ -pz)₈(μ -3,5-Me₂pz)(H₂O)}₁](C₇H₈)₅: Bu₄N-**2**(C₇H₈)₅. One pyrazolate unit of the Cu₇-ring, one dimethylpyrazolate unit of the Cu₁₄-ring and one pyrazolate unit of the Cu₉-ring are disordered

over two positions (50/50, 40/60, 40/60). A terminal CH₃ group of one of the two TBA counterions is disordered over two positions (50/50), and the carbonate ion is disordered over three positions (55/28/17). Four of the five toluene solvent molecules are disordered. Hydrogens for the water molecule could not be located from the residual electron density map.

(Bu₄N)₂[CO₃²⁻ {*cis*-Cu^{II}(μ-OH)(μ-pz)}₈ {*cis*-Cu^{II}(μ-OH)(μ-3,5-Me₂pz)}₁₄ {*cis*-Cu^{II}(μ-OH)(μ-pz)}₈]: Bu₄N-3. Only very small crystals of Bu₄N-3 could be obtained, which diffracted poorly; therefore, only preliminary data are presented here (monoclinic, P2/n, a = 23.864(4) Å, b = 14.830(2) Å, c = 31.070(4) Å, β = 95.138(10), V = 10952(3) Å³, Z = 2). Although the severely disordered solvent molecules and Bu₄N⁺ counterions are not modeled, the identity of the nanojar is established unambiguously, and all Cu-atoms are refined anisotropically (R₁ = 16%, R_w = 20%).

Table 2. Crystallographic data of nanojars Et₄N-1 and Bu₄N-2.

	Et ₄ N-1(H ₂ O) ₂ (C ₇ H ₈) ₄	Bu ₄ N-2(C ₇ H ₈) ₅
Formula	C ₁₃₂ H ₁₉₂ Cu ₂₉ N ₆₀ O ₃₄	C ₁₈₈ H ₂₉₄ Cu ₃₀ N ₆₂ O ₃₄
FW	5006.10	5873.03
Crystal system	monoclinic	triclinic
Space group	C2/c	P $\bar{1}$
a/Å	30.0687(6)	22.5542(3)
b/Å	26.6625(5)	23.0479(3)
c/Å	26.2115(5)	26.4003(3)
α/deg	90.000	90.645(1)
β/deg	117.373(1)	102.627(1)
γ/deg	90.000	118.805(1)
V/Å ³	18661.0(6)	11625.0(3)
Z	4	2
D _{calc} /g cm ⁻³	1.782	1.678
μ/mm ⁻¹	3.304	2.754
Reflns collected/unique	225664/23223	305982/41130
R(int)	0.1191	0.0587
Obsd reflns [<i>I</i> > 2σ(<i>I</i>)]	14010	30705
Data/parameters/restrains	23223/1205/34	41130/2867/57
GOF (on <i>F</i> ²)	1.063	1.034
R(<i>F</i>), R _w (<i>F</i>) [<i>I</i> > 2σ(<i>I</i>)]	0.0556, 0.1180	0.0483, 0.1296

R(F), R _w (F) [all data]	0.1201, 0.1481	0.0754, 0.1508
-------------------------------------	----------------	----------------

ACKNOWLEDGEMENTS. This material is based upon work supported by the National Science Foundation under Grant No. CHE-1404730. B.C. thanks the American Chemical Society for financial support through the Project SEED endowment.

REFERENCES

- ¹ I. R. Fernando, S. A. Surmann, A. A. Urech, A. M. Poulsen and G. Mezei, *Chem. Commun.*, 2012, **48**, 6860–6862.
- ² G. Mezei, *Chem. Commun.*, 2015, **51**, 10341–10344.
- ³ B. M. Ahmed, B. R. Szymczyna, S. Jianrattanasawat, S. A. Surmann and G. Mezei, *Chem. Eur. J.*, 2016, DOI: 10.1002/chem.201600271.
- ⁴ B. L. Jacobson and F. A. Quioco, *J. Mol. Biol.*, 1988, **204**, 783–787.
- ⁵ (a) M. Elias, A. Wellner, K. Goldin-Azulay, E. Chabriere, J. A. Vorholt, T. J. Erb and D. S. Tawfik, *Nature*, 2012, **491**, 134–137; (b) D. Gonzalez, M. Richez, C. Bergonzi, E. Chabriere and M. Elias, *Sci. Rep.*, 2014, **4**, 6636.
- ⁶ M. J. Langton, C. J. Serpell and P. D. Beer, *Angew. Chem. Int. Ed.*, 2016, **55**, 1974–1987.
- ⁷ N. Busschaert, C. Caltagirone, W. Van Rossom and P. A. Gale, *Chem. Rev.*, 2015, **115**, 8038–8155.
- ⁸ R. Dutta and P. Ghosh, *Chem. Commun.*, 2014, **50**, 10538–10554.
- ⁹ R. Custelcean, *Chem. Commun.*, 2013, **49**, 2173–2182.
- ¹⁰ I. Ravikumar and P. Ghosh, *Chem. Soc. Rev.*, 2012, **41**, 3077–3098.
- ¹¹ N. H. Evans and P. D. Beer, *Angew. Chem. Int. Ed.*, 2014, **53**, 11716–11754.
- ¹² R. Custelcean, *Chem. Soc. Rev.*, 2014, **43**, 1813–1824.
- ¹³ A. Frontera, *Coord. Chem. Rev.*, 2013, **257**, 1716–1727.
- ¹⁴ S. Lee, C.-H. Chen and A. H. Flood, *Nat. Chem.*, 2013, **5**, 704–710.
- ¹⁵ N. Lopez, D. J. Graham, R. McGuire Jr., G. E. Alliger, Y. Shao-Horn, C. C. Cummins, D. G. Nocera, *Science*, 2012, **335**, 450–453.
- ¹⁶ R. B. P. Elmes and K. A. Jolliffe, *Chem. Commun.*, 2015, **51**, 4951–4968.
- ¹⁷ P. A. Gale, C. Caltagirone, *Chem. Soc. Rev.*, 2015, **44**, 4212–4227.
- ¹⁸ A. Caballero, F. Zapata, P. D. Beer, *Coord. Chem. Rev.*, 2013, **257**, 2434–2455.
- ¹⁹ S.-K. Ko, S. K. Kim, A. Share, V. M. Lynch, J. Park, W. Namkung, W. Van Rossom, N. Busschaert, P. A. Gale, J. L. Sessler and I. Shin, *Nat. Chem.*, 2014, **6**, 885–892.
- ²⁰ P. A. Gale, R. Pérez-Tomás and R. Quesada, *Acc. Chem. Res.*, 2013, **46**, 2801–2813.
- ²¹ J. A. Cooper, S. T. G. Street and A. P. Davis, *Angew. Chem. Int. Ed.*, 2014, **53**, 5609–5613.
- ²² N. Busschaert and P. A. Gale, *Angew. Chem. Int. Ed.*, 2013, **52**, 1374–1382.
- ²³ A. Vargas Jentzsch and S. Matile, *Top. Curr. Chem.*, 2015, **358**, 205–240.
- ²⁴ Y. Marcus, *Ion Properties*, Marcel Dekker, New York, 1997.
- ²⁵ P. A. Angaridis, P. Baran, R. Boča, F. Cervantes-Lee, W. Haase, G. Mezei, R. G. Raptis and R. Werner, *Inorg. Chem.*, 2002, **41**, 12219–2228.

- ²⁶ G. Mezei, M. Rivera-Carrillo and R. G. Raptis, *Inorg. Chim. Acta*, 2004, **357**, 3721–3732.
- ²⁷ G. Mezei, M. Rivera-Carrillo and R. G. Raptis, *Dalton Trans.*, 2007, 37–40.
- ²⁸ L. Mathivathanan, M. Rivera-Carrillo and R. G. Raptis, *Inorg. Chim. Acta*, 2012, **391**, 201–205.
- ²⁹ G. Mezei and R. G. Raptis, *Inorg. Chim. Acta*, 2004, **357**, 3279–3288.
- ³⁰ W. Henderson and J. S. McIndoe, *Mass Spectrometry of Inorganic and Organometallic Compounds*, Wiley, 2005, pp. 117–119.
- ³¹ I. R. Fernando, N. Daskalakis, K. D. Demadis and G. Mezei, *New J. Chem.*, 2010, **34**, 221–235.
- ³² E. Quartapelle Procopio, F. Linares, C. Montoro, V. Colombo, A. Maspero, E. Barea and J. A. R. Navarro, *Angew. Chem. Int. Ed.*, 2010, **49**, 7308–7311.
- ³³ S. Su, Y. Zhang, M. Zhu, X. Song, S. Wang, S. Zhao, S. Song, X. Yang and H. Zhang, *Chem. Commun.*, 2012, **48**, 11118–11120.
- ³⁴ W. G. Mook, *Chemistry of carbonic acid in water*, in *Environmental Isotopes in the Hydrological Cycle: Principles and Applications*, Vol. 1, IAEA / UNESCO: Paris, 2001, pp. 87–98.
- ³⁵ T. A. Crowell, C. D. Jones and A. J. Shuker, US Patent 6046227, 2000.
- ³⁶ G. A. Eller and W. Holzer, *Molbank*, 2006, **2006**, M464.
- ³⁷ K. England, H. Mason, R. Osborne and L. Roberts, *Tetrahedron Lett.*, 2010, **51**, 2849–2851.
- ³⁸ M. K. Ehlert, S. J. Rettig, A. Storr, R. C. Thompson and J. Trott, *Can. J. Chem.*, 1991, **69**, 432–439.
- ³⁹ K. P. Maresca, D. J. Rose and J. Zubieta, *Inorg. Chim. Acta*, 1997, **260**, 83–88.
- ⁴⁰ K. Takagi, A. Bajnati and M. Hubert-Habart, *Bull. Soc. Chim. France*, 1990, **127**, 660–666.
- ⁴¹ H. Bredereck, R. Sell and F. Effenberger, *Chem. Ber.*, 1964, **97**, 3407–3417.
- ⁴² C. S. Rondestvedt, Jr. and P. K. Chang, *J. Am. Chem. Soc.*, 1955, **77**, 6532–6540.
- ⁴³ T. Ruman, Z. Ciunik and S. Wolowiec, *Polyhedron*, 2003, **22**, 581–586.
- ⁴⁴ B. M. Ahmed, H. Zhang, Y. Mo and G. Mezei, *J. Org. Chem.*, 2016, **81**, 1718–1722.
- ⁴⁵ G. Yang and R. G. Raptis, *Inorg. Chim. Acta*, 2003, **352**, 98–104.
- ⁴⁶ A. Maspero, G. B. Giovenzana, D. Monticelli, S. Tagliapietra, G. Palmisano and A. Penoni, *J. Fluorine Chem.*, 2012, **139**, 53–57.
- ⁴⁷ N. Kitajima, K. Fujisawa, C. Fujimoto, Y. Moro-oka, S. Hashimoto, T. Kitagawa, K. Toriumi, K. Tatsumi and A. Nakamura, *J. Am. Chem. Soc.*, 1992, **114**, 1277–1291.
- ⁴⁸ J. Olguín and S. Brooker, *New J. Chem.*, 2011, **35**, 1242–1253.
- ⁴⁹ D. L. Reger, J. R. Gardinier, T. C. Grattan, M. R. Smith and M. D. Smith, *New J. Chem.*, 2003, **27**, 1670–1677.
- ⁵⁰ R. G. Jones and M. J. Mann, *J. Am. Chem. Soc.*, 1953, **75**, 4048–4052.
- ⁵¹ B. M. Ahmed and G. Mezei, *RSC Adv.*, 2015, **5**, 24081–24093.
- ⁵² APEX2 v2014.9-0; Bruker AXS Inc.: Madison, WI, 2014.